# Building Model Systems to Understand Proton-Coupled Electron Transfer in Heme: Spectroscopic Investigation of Charge Transfer to Axially Bound Diimide Acceptors
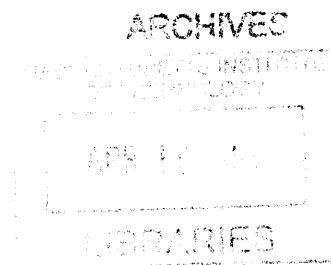
By

Christina J. Hanson

B.S. Chemical Physics
University of California at San Diego, 2008

SUBMITTED TO THE DEPARTMENT OF CHEMISTRY IN PARTIAL FULFILLMENT
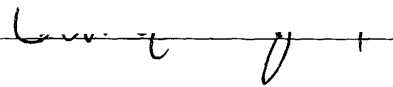OF THE REQUIREMENTS FOR THE DEGREE OF

MASTERS OF SCIENCE IN INORGANIC CHEMISTRY
AT THE

MASSACHUSETTS INSTITUTE OF TECHNOLOGY

February 2013
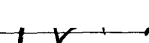
Signature of Author: _____

Department Of Chemistry

February 18, 2013

Certified By: _____

Daniel G. Nocera

Henry Dreyfus Professor of Energy

Thesis Advisor

Accepted By: _____

Robert W. Field

Robert T. Haslam and Bradley Dewey Professor of Chemistry

Director of Graduate Studies

*For my parents, espeically my mother, whose unwavering and positive love and support is greatly missed*

Building Model Systems to Understand Proton-Coupled Electron Transfer in Heme:
Spectroscopic Investigation of Charge Transfer to Axially Bound Diimide Acceptors
By
Christina J. Hanson

Submitted to the department of Chemistry
On February 18 2013 in Partial Fulfillment of the
Requirements for the
Degree of Masters of Science in Chemistry.

## ABSTRACT

Proton-Coupled Electron Transfer (PCET) is an important mechanistic motif in chemistry, which allows for efficient charge transport in many biological systems. We seek to understand how the proton and electron motions are coupled in a bidirectional system allowing for individual turning of the kinetics and thermodynamics. The target of interest is a biomimedic heme system allowing for a detailed mechanistic study of the formation of the oxidation states of heme, of particular interest the highly reactive $Fe(IV)=O$ species. The bidirectional model is prepared using a hangman porphyrin with an axially coordinated to the metal center, and the electron transfer event is triggered by excitation of the porphyrin. The synthesis of this motif is discussed as well as initial studies into the binding of a coordinated electron acceptor to the metal center. In the future, the excited state of the acceptor will be used to trigger the electron transfer portion of the PCET event. To understand the signatures of different electron acceptors and binding to the metal center, a redox inactive zinc porphyrin is used as a model to allow for longer excited state lifetimes and well known transient signatures. Three diimide acceptors have been coordinated through a pyridine ring to the metal center of the porphyrin, and electron transfer was triggered both by excitation of the porphyrin and the acceptor. Lifetimes of the charge separated state were determined using picoseconds and nanosecond transient absorption. The acceptors are then coordinated to a symmetrical iron porphyrin in an attempt to understand the behavior of charge separation in the more complicated open d shell system. Spectroscopic data of both systems is shown.

Thesis Supervisor: Daniel G. Nocera
Title: Henry Dreyfus Professor of Energy

# Table of Contents

**Chapter 1:** Principles of Proton-Coupled Electron Transfer

**Chapter 2:** Synthesis of Iron Hangman Porphyrin Library

**Chapter 3:**  Defining Important Experimental Parameters Using Nanosecond

Transient Absorption Spectroscopy

**Chapter 4:** Ultrafast Photoinduced Charge Separation and Charge Recombination of

Axially Bound Diimide Electron Acceptors to ZnTPP

**Chapter 5:** Future Directions

# List of Figures and Schemes

# Chapter 1

# Principles of Proton-Coupled
# Electron Transfer

## 1.1 Motivation and theory

Proton-Coupled Electron Transfer (PCET) is a complex and important mechanistic motif in biology and chemistry, as many processes that utilize chemical energy and bioenergy conversion are fundamentally PCET in nature. PCET defined simply is the coupled movement of electrons to the molecular motions of protons.[1] Our current understanding of PCET is based on theoretical calculations,[2,3] measurements of electron transfer rates in biological systems,[4] and model systems.[5-7] The work of this thesis attempts to build a model system that provide insight into the intricate details of bidirectional PCET, in which the proton and the electron move along different pathways, allowing for their kinetics and thermodynamics to be intricately tuned.

Model systems are advantageous as they allow for i) the direct isolation of the PCET process, ii) can be modified to precisely control the distances for transfer of the electron (ET) and proton (PT) independently, iii) can be electronically tuned to achieve the best possible environment for the PCET event, and iv) can be studied using transient spectroscopic techniques that allow direct insight in to the timescales of transfer. The work described herein seeks to understand how modifications to redox potentials and spectral properties of the system promote or inhibit charge transfer (CT) processes.

## 1.2 PCET in nature

In 1961 Peter Mitchell recognized the importance of PCET in biology with the observation that during oxidative and photosynthetic phosphorylation the movement of protons of was driven by the ET.[8] Subsequent work has shown PCET to be an important contributing mechanism to many biological processes, including, but not limited to,

13

small molecule activation, proton pumps, radical initiation, and oxygen transport.[4,9,10] As a consequence, experiments that probe the fundamental principles of PCET will not only provide insight into a deeper understanding of the nature of complicated biological processes, but also potentially direct scientists towards targeted drug design.[11,12]

Ribonucleotide Reductase (RNR) is a biological system that derives its function from PCET.[9,13–18] RNR is the rate-limiting enzyme in the DNA chain, and therefore there is great interest into understanding the fundamental mechanisms of the RNR radical transport chain. This information is vital to designing therapeutics that target a variety of cancers,[19] myeloproliferative diseases,[20,21] and suppression of tumorigenic factors.[22] RNR has one of the longest PCET distances in biology, spanning 2 subunits at 35 Å. Subunit $\alpha 2$ contains the enzyme active site while subunit $\beta 2$ contains the active diiron-tyrosyl radical cofactor. In this protein manifold, it is postulated that the proton and the electron, and hence the amino acid radical, is delivered along a PCET radical hopping pathway. From information gathered from the crystal structure, it is known that a series of tyrosine (Y) and tryptophan (W) amino acids are found along the transport chain. Depending on the protonation of the residue, these amino acids can have redox states that can foster the movement of the electron and proton along the chain. (Figure 1.1a)

Recent work using unnatural fluorotyrosine residues and a ruthenium bipyridine photooxidant has provided insight into the complex mechanism of radical injection into the $\alpha$ subunit of the protein.[18] The experiment underscores the importance of each individually placed tyrosine in the transport chain– remove one of the residues, specifically Y730, and the radical transport shuts down. This is believed to be a direct result of a hydrogen bond network between Y731 and Y730 that allows for a colinear proton transfer

14
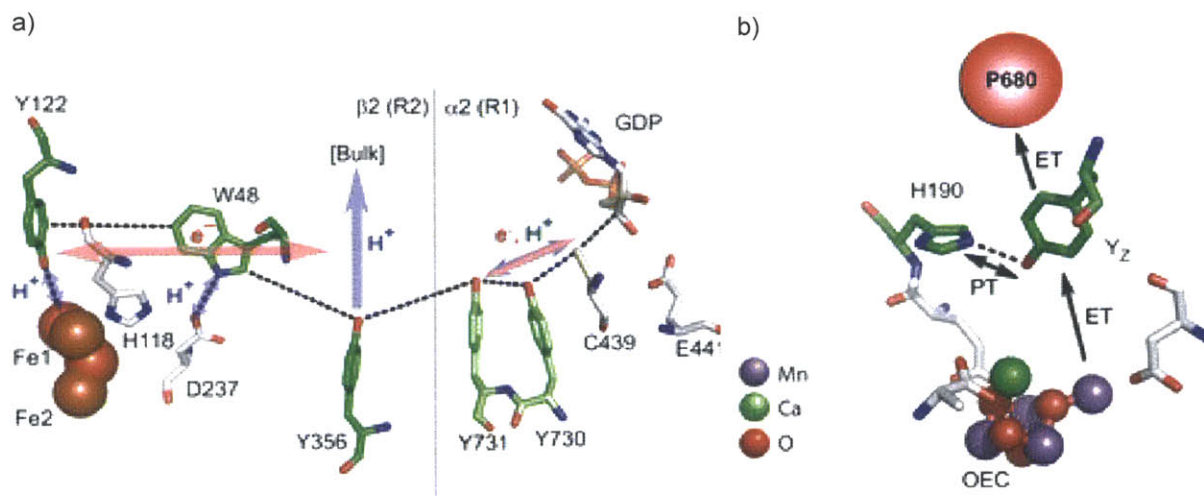
**Figure 1.1:** Examples of PCET in biological systems a) RNR pathway in both α2 and β2 subunits. The pathways for both the electron and the proton are shown. As described in the text the electron must manage a very long transfer distance while coupled to many protons along the transport chain. b) PCET in Photosystem II, again a very long ET distance is coupled to a much smaller PT transfer distance. Figure adapted from Reece and Nocera Annu Rev Biochem 2009 78 673-99.

pathway. Without this hydrogen bond, PCET to shuttle the radical to α2 is not possible.

It has been proposed that enzymes such as cytochrome P450 and cytochrome c oxidase also operate via PCET pathways in order to avoid high-energy intermediates associated with the stepwise process.[23,24] The ability to make accurate model systems of these and other biologically important PCET systems is extremely useful. For example, it is known that enzyme cofactors manage long charge transport distances with bidirectional PCET and as such, extremely large isotope effects have been found upon substrate activation in lipoxygenase and cofactors of other enzymes.[25,26] This suggests that the proton transfer distance is a key determinant of the PCET process that leads to the large isotope effects. To evaluate this contention, if model systems can be designed such that the distance of the proton can be carefully controlled, then the extent to which the proton and the electron are coupled can be probed directly and isotope effects can be isolated and explained in these enzyme classes.

Another PCET process that has generated a large amount of interest is the water splitting mechanism of the oxygen evolving catalyst (OEC) in Photosystem II (PSII). In short, light is absorbed by PSII and the holes of the current generated are transported to the OEC where water is oxidized to $O_2$. The electrons from the system are fed into Photosystem I (PSI) where, with additional light capture, NADP is reduced to NADPH by a reductase. With efficient shuttling of protons and electrons, the OEC is able to store enough equivalents to run the four proton/four electron water splitting process. It is believed that the key to chemical alternative energy solutions can be found if a thorough understanding of the water oxidation process of the OEC is achieved. The Nocera lab has developed a catalyst of Co(II) and phosphate, that at neutral pH is believed to undergo a similar mechanism to that of the OEC to split water so the $H_2$ and $O_2$ can be stored as fuel (Figure 1.1b).

## 1.3   Building PCET theory from the ground up

In order to understand the intricate aspects of PCET, it is valuable to first examine the fundamental motions of the lighter particle, the electron. The transfer of the electron has is described by Marcus theory.[27–29] Marcus Theory can then be modified with non-classical treatments to describe the motion of the proton, thus allowing a comprehensive theory of PCET to be developed.

### 1.3.1 ET is understood: Marcus theory

The theory for ET processes was first described by Rudolf Marcus[27,28,30] and Norman Hush[31,32] in the 1950s and has been extended to numerous systems using quantum mechanical corrections.[29,33] Marcus' initial contribution recognized that ET between an

16

electron donor (De) and electron acceptor (Ae) is directly coupled to a solvent coordinate that drives the charge transfer (CT) process. The polarization of the solvent will change during the course of the ET event to stabilize the De and the Ae while the charge from the electron transfer is redistributed (Figure 1.2). This linear treatment of the solvent coordinate allows for the product and reactants to be mapped as intersecting parabolas defined by the specific solvent coordinate, and leads to a simplification of the Arrhenius equation for rate crossing from product to reactant surfaces (Figure 1.3a). The rate of non-adiabatic ET ($k_{ET}$) can be described by the semi-classical Marcus-Levich expression:[29,33]

$$k_{ET} = \sqrt{\frac{\pi}{\hbar^2 \lambda k_B T}} |V_{el}|^2 \exp\left[-\frac{(\Delta G^\circ + \lambda)^2}{4\lambda k_b T}\right] \qquad \text{(eq 1.1)}$$

The key parameters include i) The reorganizational energy of the system ($\lambda$) including the nuclear and solvent reorganization, ii) The thermodynamic driving force ($\Delta G^\circ$) associated with the redox event, and iii) the electronic coupling matrix ($V_{el}$) between the product and reactant at the crossover point. It is important to note that $V_{el}$ decays exponentially with increasing distance between reactant and product, reflecting the lack of wavefunction overlap that results with decreasing interaction between the De and Ae.

The Marcus theory predicts three major regimes in which ET takes place, the "normal" regime, in which $k_{ET}$ increases with increasing $-\Delta G^\circ$, the "top" regime in which $k_{ET}$ is at a maximum and $-\Delta G^\circ = \lambda$, and the "inverted" regime, in which $k_{ET}$ decreases as $-\Delta G^\circ > \lambda$ (Figure 1.3b). Much attention has been paid to the latter regime, as experimental evidence was obtained almost 20 years after Marcus'
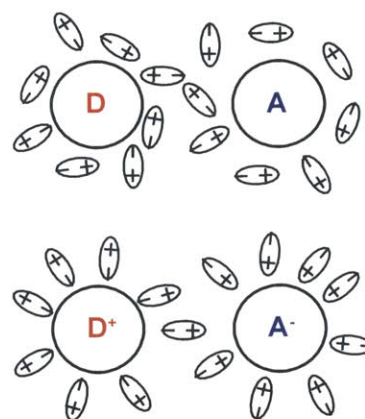
Figure 1.2: Solvent reorganization during an ET event to stabilize the reactant and product.

17

prediction[34] utilizing techniques that specifically isolate the ET event from any other kinetics processes (such as diffusional kinetics). The ability to probe ET with lasers to conduct time resolved experiments using excited state redox systems has verified the importance of Marcus theory and the inverted regime in biological systems,[35-39] photosynthetic systems,[35-37] and energy capture and storage.[43-45] Previous work, particularly the work by Harry Gray pioneered the use of covalently bound excited state redox systems that are able to store excess energy in the excited state, which allows ET to be thermodynamically accessible either directly or through a sacrificial quencher ('flash-quenching' which is described in detail elsewhere[17,18]).[35-37] Most importantly, this method takes a pre-arranged De|Ae ground state system in a fixed geometry that, when triggered with a laser pulse, will undergo intramolecular ET. Upon the absorption of a photon, an electron is promoted from the excited state of De to Ae, which can be kinetically resolved in real time by transient absorption (TA) or transient emission (TE) spectroscopy on a very fast (ps) timescale. These methods have offered great insight into the development of many systems including but not limited to photovoltaics,[44,46-48] chemosensing,[49,50] and
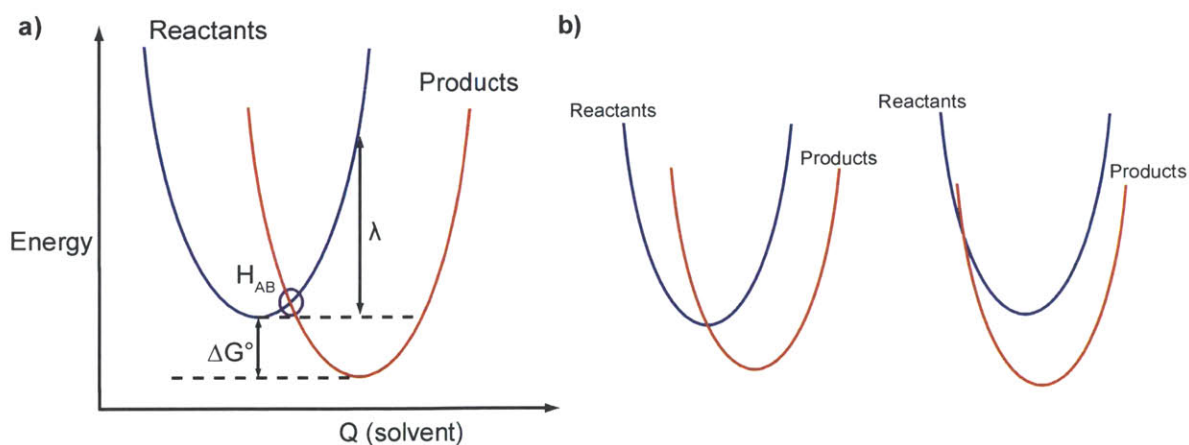


**Figure 1.3:** Marcus paraboals representing the potential wells for ET between donor and acceptor. a) Potential wells for D and A showing all relevant variables. b) normal ET regime and inverted regime.

batteries.[51]

The methods for understanding ET have been well developed, so it follows that some of these techniques can be used to study more complex PCET systems in which the motion of the proton is coupled to the motion of the electron.

### 1.3.2 Tackling the complexity of PCET

As with ET, proton transfer (PT) involves the controlled movement of the proton from the donor (Dp) to the acceptor (Ap). The PT movement affects $V_{el}$, $\lambda$, and $\Delta G^\circ$ expressed in Eq. 1.1. The PCET process can be visualized by the square scheme in Figure 1.4. As the proton moves, the electrochemical potentials of the substrate change, and thus the movement of the electron is affected. Alternatively, as the electron moves, the pKa of the system changes, and the movement of the proton is affected. If the reaction follows the border of the square scheme, it undergoes a stepwise process (ETPT or PTET) and forms a high-energy intermediate state that may thermodynamically prevent the reaction from proceeding. If the reaction however follows a concerted PCET process, represented as any pathway traveling through the center of the square, the movements of the proton and the electron are coupled, preventing the existence of a high-energy transition state. The extent to which the electron and the proton are coupled can vary within the area of the square, however it is assumed that any coupling avoids a high-energy intermediate.

Theoretical treatments of PCET by Cukier[1,52,53] and Hammes-Schiffer[54-57] suggest a two dimensional approach to traditional Marcus Theory. The model creates two sets of intersecting parabolas. There is a specific contribution of the proton coordinate to both $\lambda$ and $\Delta G^\circ$, and a vibronic coupling term that is the summation of Frank Condon overlaps of
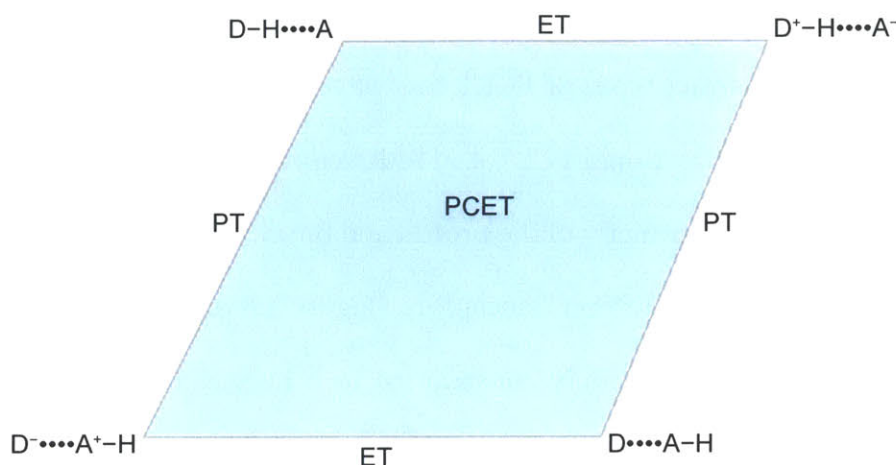
**Figure 1.4:** Square scheme representing the stepwise Et and PT processes (around the edge0 and the concerted process (shaded aread in the middle)

the Dp and Ap vibrational states. The model is inherently more complicated, as now $k_{PCET}$ depends not only on the parameters for ET, but the pKa, proton-solvent interactions, and the reorganization energy associated with the proton movement.

As such, system design also plays a large role in the $k_{PCET}$ and efficiency of transfer. PCET comes in two distinct forms. In the first, sometimes referred to as "unidirectional" PCET ("Hydrogen Atom Transfer" (HAT) is a limiting form[9,58,59]) the proton and the electron travel along the same coordinate to either the same or different acceptors (Figure 1.5a). The second type, usually referred to as "bidirectional" PCET, utilizes different acceptors for both the proton and the electron (Figure 1.5b). In this case, the proton and the electron are traveling separately through space. Owing to the fact that PCET is inherently a quantum mechanical process, both the proton and the electron must tunnel, however (at a fixed energy) the proton has a wavelength that is ~40 times smaller than that of the electron. Therefore the distance that the proton can travel is extremely limited compared to the electron.

### 1.3.3 Flavors of PCET: Unidirectional PCET

There are two distinct types of PCET that have been studied both by native and model systems,[13,58,59] unidirectional PCET and bidirectional PCET. Unidirectional PCET is characterized by colinear transfer of the proton and the electron, usually from the same donor to either the same or different acceptors (Figure 1.5a). For either configuration of acceptors, the proton is generally constrained to a hydrogen bond distance, while the electron can travel over much longer distance. This is a direct consequence of the fact that the proton has a much larger mass than the electron, so it tunnels over a much shorter distance. One limit of unidirectional PCET is Hydrogen Atom Transfer (HAT), in which the electron and the proton travel together as a hydrogen atom radical to the same acceptor. Hammes-Schiffer has recently outlined theoretical classifications for PCET with a classification that represents the system by electron–proton mixed vibronic states.[60] If the splitting between the ground and first excited vibronic state is larger than $k_B T$ (thermal energy) then the transfer occurs completely on the ground vibronic state and the reaction is considered *vibronically adiabatic*. Transfers that are vibronically adiabatic are considered to be only purely adiabatic HAT transfers, and therefore there are very few systems that are considered to be this type.

As the difference between the distance that the proton and the electron travels grows, the system becomes *vibronically nonadiabatic* and begins to involve excited states because the splitting between the ground and excited states is smaller than $k_B T$. These systems are generally *electronically nonadiabatic*, meaning that the movement of the electron through the hydrogen bond depends directly on proton fluxuations. Therefore, the rate at which the proton tunnels is usually *less* than that of the electron tunneling,

and small fluxuations in the movement of the proton can induce transfer of the electron. These systems are more common than the truly adiabatic HAT systems described above. Hammes- Schiffer goes so far as to suggest that there are very few PCET systems that fit the adiabatic HAT criteria.[60] For the purposes of this thesis, any colinear transfer of a proton and an electron will be considered unidirectional PCET. Chemical examples of unidirectional systems include both entirely organic systems[58,61,62] and inorganic systems.[63,64] Additionally, it has be proposed by Babcock and others that one of the most important steps in Photosystem II, the oxidation of the $CaMn_2$ cluster by a tyrosyl radical $Y_z^{\bullet}$, is a HAT process to avoid a high-energy intermediate.[59,65,66]

The study of model systems to understand complex PCET events in biology and nature was initiated by the unidirectional model system designed by Turro and Nocera shown in Figure 1.5a.[67] The system was based on earlier fixed distance ET studies and attached a proton donor/acceptor hydrogen bond interface, consisting of a carboxylic acid dimer, on one of the β-pyrrolic positions of an electron donating Zinc(II) porphyrin. The other side of the carboxylic acid dimer was attached to an electron acceptor (3,4,dinitrobenzene). Photoinduced PCET was triggered from the prophyrin excited state and the PCET kinetics in a non-polar, non-hydrogen bonding solvent were determined by TA and TE . Additionally, the extent to which the proton and the electron are coupled were determined from deuterium isotope experiments, which determined that the extent of coupling is minimal due to the symmetric nature of the hydrogen bond scaffold. Ensuing studies incorporated asymmetric hydrogen bond interfaces utilizing an amidinium-carboxylate bridge, which loosely mimics the arginine-aspartate salt bridge that is an important structural aspect of many biological systems.[68,69] Additional studies

were performed to understand the importance of the placement of the hydrogen bond bridge on the porphyrin and the affects of rotation and ionization of the bridge on the rate of PCET.[70-72]

## *1.3.4 Flavors of PCET: Bidirectional PCET*

Of greater interest to the work in this thesis is bidirectional PCET in which the proton and electron acceptors are separated in space, allowing for a very long ET distance compared to the shorter PT distance (Figure 1.5b). In such constructs, the electron and proton can travel along different pathways, allowing for very long electron tunneling distances compared to the shorter distance necessary for proton tunneling. As long as the thermodynamics and kinetics of an electron depend on the position of a specific proton or
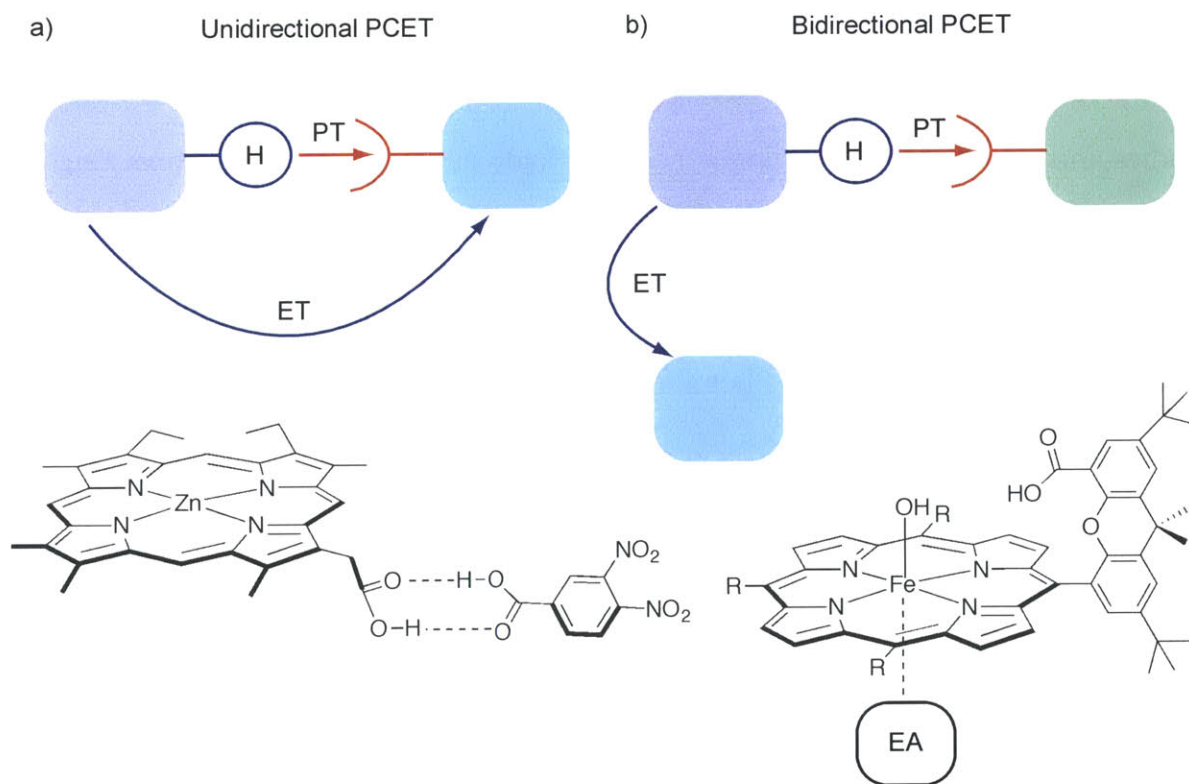


**Figure 1.5:** Different PCET orientations a) Unidirectional, in which the electon and the proton travel along the same coordinate to one acceptor. b) bidirectiona PCET in which the proton and the electron travel along different coordinates to different acceptors

a set of specific protons at any moment in time, direct coupling will occur. This suggests that the electron need not be coupled to the *same* proton throughout the transfer, an important implication for many biological bidirectional PCET systems. Hammes-Schiffer defines this regime as *vibronically nonadiabatic* and *electronically adiabatic* suggesting that the electrons may not respond instantaneously to the movement of the proton, and the coupling is described as the product of the electronic coupling of the ET states and the overlap of the proton vibrational wavefunctions of the reactants and products.[60] More simply, when the electron is localized on the De, the lowest energy state for the proton is near the Dp, when the electron is more localized on the Ae, the lowest energy level for the proton is near the Ap.

Bidirectional PCET is a fundamental pathway for transfer of protons and electrons in many biological constructs and chemical reactions thus providing an imperative to build model systems that allow for thorough investigations of the PCET process. Model systems afford for a large amount of flexibility in experimental design, as many conditions and constructs can be tested to define the limitations of the native process. For bidirectional systems in particular, the system is inherently modular because the ET distance and PT distance can be tuned independently. This design flexibility is crucial because it helps towards building an understanding of the extent to which the proton and the electron couple through the PCET process.

There have been many theoretical and experimental efforts that seek to understand the intricate details of bidirectional PCET in chemical and biological systems, specifically in enzymatic catalytic reactions. The most well known example in the literature is Photosystem II, where water oxidation at one site and light absorption at a distant

chlorophyll antenna array are coupled. PCET is used to shuttle holes between the oxidized porphyrin ($P_{680}$) and the $[Mn]_4$ cluster of the OEC. To drive the transfer, a (Tyrosine) Y161-H190 (Histidine) pair is oxidized by $P_{680}$ to generate Y•, at the same time that a proton dissociates from the Y and is transferred to the H. This process is then reversed upon oxidation of the $Mn_4Ca$ cluster in the OEC, and the proton is transferred back to the Y. This "rocking mechanism" of the proton is repeated as electrons are shuttled across the orthogonal pathway. In order for the PCET event to occur, the $H_{190}$ must be precisely placed in the system to shuttle the proton. Additionally, at least 5 other PCET processes have been identified in Photosystem II, ranging in time scales from ps to ms. Each event requires precise distance tuning of the proton and the electron to be successful, and therefore many model systems, crystal structures, and native systems have been studied to try and build a complete understanding of this intricate process.[73]

Hammarström et. al. showed that a Tryptophan (W) linked to a photooxidant, $Ru^{II}(bpy)_3$, can undergo either stepwise proton and electron transfer, a pH independent process, or PCET, a pH dependent process, with water as the designated proton acceptor in both cases. Using a flash-quench method, the different pathways for PCET and stepwise transfer could be determined using TA spectroscopy, as the signals for the formation of W•H⁺ or W• are distinguishable. Theory has suggested that the process can only proceed via the concerted process, which is considered the dominate process of many Y systems because PT is unfavorable based on the comparison of the pKas in various systems with water as the acceptor. Hammarström has shown that, in general the PCET mechanism for amino acids in water dominates, especially in the case of Y systems, however these systems can be carefully tuned to undergo the stepwise process, suggesting that more

intensive studies are necessary to completely understand these intricate mechanisms.[74]

## 1.4 Model systems

The Nocera group has been working to develop model systems to study biological processes that are believed to be PCET events. We have developed model systems for both subunits of RNR, in order to understand the electron and proton transfer pathways as well as model systems of the heme found in enzymes such as cytochrome $c$ and cytochrome P450. The latter will be the focus of this work, as the interconversion of the $Fe^{II}$, $Fe^{III}$, and $Fe^{IV}$ oxidation states of heme during the formation of Compound I (Cpd I) $(P^{\cdot+})Fe^{IV}=O$ and Compound II (Cpd II) $(PFe^{IV}=O)$. By building systems that model the heme environment we have the ability to precisely control the proton and electron transfer distances to understand to what extent the proton and the electron couple as well as determine $\lambda$ and $\Delta G°$ for the system. We believe that controlled kinetic studies can be conducted on model compounds utilizing TA. Our model to study PCET is the hangman porphyrin (HPX) (Figure 1.5b) in which the coordinates of the proton and the electron can be individually tuned.

### 1.4.1 Previous generation models

Our current understanding of bidirectional PCET is based on work performed previously by Justin Hodgkiss and Alexander Krivokapić in our group.[75] A donor–acceptor (D–A) system that included the Fe-HPX scaffold as the electron acceptor and a zinc porphyrin (ZnP) as an electron donor was synthesized. ZnP was chosen because it has known spectroscopic signatures, a favorable redox potential (+0.85 V vs. SCE)[76] to reduce $Fe^{III}$HPX, and contains a redox inactive metal. In an impressive synthesis, they

26
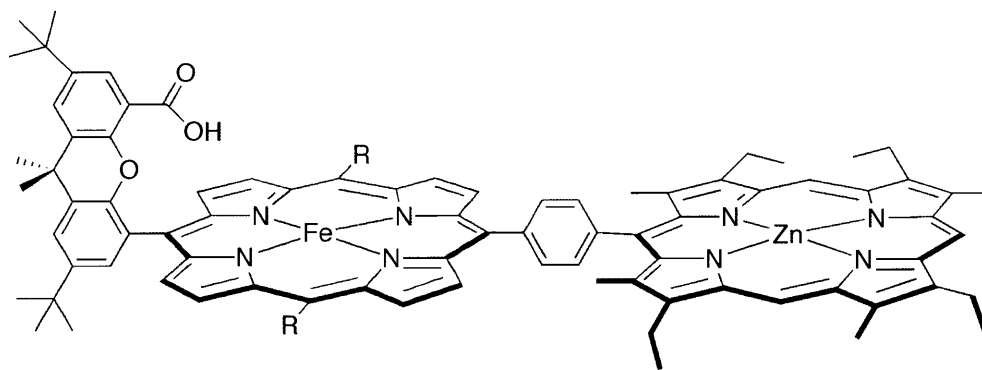
**Figure 1.6:** Bidirectional system previously explored in the Nocera lab. Because of the long transfer length, energy transfer beat out electron transfer as described in the text.

covalently attached the ZnP to the porphyrin *meso* position and used its excited state to donate an electron into the FeHPX (Figure 1.6).

It is known that the ligand environment of five-coordinate iron determines the fate of the $^1$ZnP excited state.[77] Low spin iron centers—coordinated by a strong field (SF) ligand—support electron transfer, but high spin iron species—coordinated by a weak field (WF) ligand—favor energy transfer and intersystem crossing (ISC). The five-coordinate HPX scaffold with a WF hydroxyl ligand is high spin; in order for electron transfer to be the dominant relaxation pathway, the system must be coordinated with a sixth SF ligand. Justin and Alexander studied these mixed (SF/WF) systems using two SF ligands, 1-methylimidazole and 1,5-dicyclohexylimidazole. Charge separation was never observed because the ZnP excited state was quenched by either of three mechanisms: ISC to $^3$ZnP, Förster Resonance Energy Transfer (FRET), and Dexter Energy Transfer (DET). Initially, it was assumed that the lack of charge transfer was directly related to the distance dependences for energy transfer ($k_{FRET} \alpha \; r^{-6}$, $k_{DET} \alpha \; e^{-2r}$) and electron transfer ($k_{ET} \alpha \; e^{-r}$ at long distances).[78] To avoid energy transfer, the distance between donor and acceptor was decreased, but electron transfer was still not observed. They interpreted this to indicate

a large influence of the reorganizational energy required for charge separation.[1] Density functional theory (DFT) calculations show that $Fe^{III}$ rests 0.538 Å above the porphyrin plane, whereas $Fe^{II}$ or $Fe^{IV}$ are only displaced by 0.190 Å.[75] Electrochemical experiments further established that the reorganizational energy required to oxidize $TMPFe^{II}-OH_2$ to $TMPFe^{III}-OH$ is 0.61 V.[79] Therefore, although a SF ligand was axially coordinated, and the Zn donor supplied a favorable driving force, we believe that the reorganizational energy barrier prevented electron transfer. This underscores the importance of electron donor/acceptor design, as they must provide a large driving force to trigger PCET and overcome reorganization energy.[75]

## 1.4.2 Developing new model systems

A model to study the interconversion of $Fe^{III}$ to either $Fe^{II}$ or $Fe^{IV}$ are outlined in Figure 1.7. We first target an understanding of the conversion of $Fe^{III}$ to $Fe^{IV}$ because high valent metal oxos are highly reactive and prevalent in biology.[80] In order to increase the
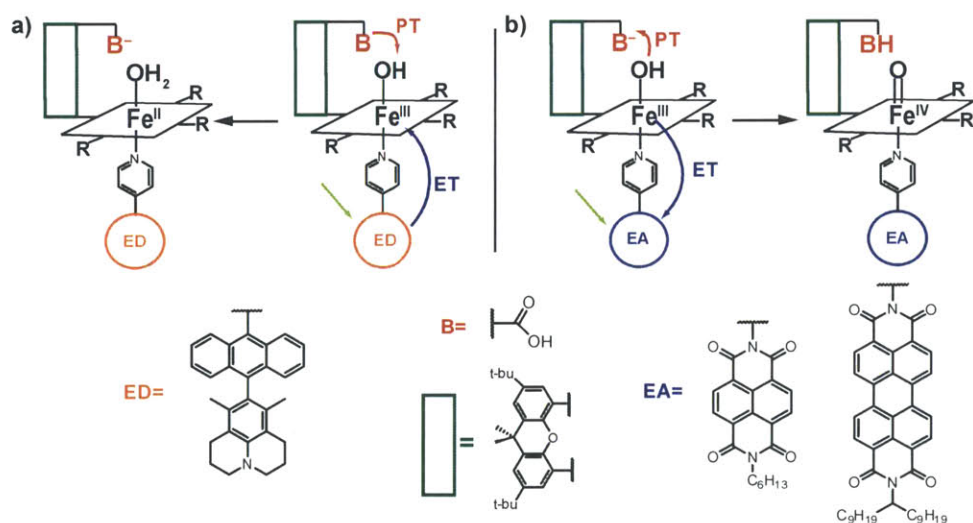


**Figure 1.7:** New model systems to be studied. These can be studied in both the forward ($Fe^{III}-->Fe^{IV}$) and the reverse ($Fe^{III}-->Fe^{II}$) directions depending on if an electron donor (ED) or an electron acceptor (EA) is used

28

driving force for PCET in such the model system, we have turned to higher reduction potential acceptors in proximity to the iron center. FeHPX has an extremely short excited state lifetime (~30 ps)[81] so excitation of the porphyrin to initiate electron transfer will likely prove ineffective. Instead, an axially coordinated electron acceptor (EA) (or electron donor, ED, for the $Fe^{II}$ case) is intended for excitation by a laser pulse. The transient excited state is designed to initiate electron transfer from the FeHPX to the EA. Since proton transfer is coupled to the oxidation of iron center, we can monitor how the hydrogen bond network changes the rate constant for electron transfer. The proton acceptor is positioned by the pendant-hanging group, which can be changed synthetically. The system is extremely modular; the proton and electron acceptors can be modified independently. Additionally, the steric and electronic environment around the metal center can be controlled by systematically varying the *meso* substituents of the porphyrin.

## *1.5 Thesis outline*

Chapter 1 has provided the motivational background for the work conducted in this thesis. Chapter 2 describes the current synthetic methods used to obtain the FeHPX system in high yields as well as initial binding studies to test the feasibility of the new dyad design. Chapter 3 reports the measurement of charge transfer using a model system of the FeHPX model system. The donor in this case is ZnTPP and with the use of a polar solvent, CT events on a ns-μs can be evaluated. Chapter 4 details the ultrafast TA experiments to understand CT events in a non-polar solvent on the three different accpetors that have been synthesized. Binding studies of the dyad and a full Marcus analysis of the ET is included. Chapter 5 describes some preliminary experiments performed in which the

acceptor was photoexcited, both in the ZnTPP system and in the corresponding FeTPP

system and charts a course for the future development of other dyad systems.

## 1.6  References

(1)   Cukier, R. I.; Nocera, D. G. *Annu Rev Phys Chem* **1998**, *49*, 337–369.

(2)   Hammes-Schiffer, S.; Stuchebrukhov, A. A. *Chem. Rev.* **2010**, *110*, 6939–6960.

(3)   Cukier, R. I. *BBA-Bioenergetics* **2004**, *1655*, 37–44.

(4)   Dempsey, J. L.; Winkler, J. R.; Gray, H. B. *Chem. Rev.* **2010**, *110*, 7024–7039.

(5)   Hammarström, L.; Styring, S. *Phil. Trans. R. Soc. B* **2008**, *363*, 1283–1291.

(6)   Mayer, J. M.; Rhile, I. J. *BBA-Bioenergetics* **2004**, *1655*, 51–58.

(7)   Miyazaki, S.; Kojima, T.; Mayer, J. M.; Fukuzumi, S. *J. Am. Chem. Soc.* **2009**, *131*, 11615–11624.

(8)   Mitchell, P. *Nature* **1961**, *191*, 144–148.

(9)   Reece, S. Y.; Nocera, D. G. *Annu Rev Biochem* **2009**, *78*, 673–699.

(10) Chang, C. J.; Chang, M. C. Y.; Damrauer, N. H.; Nocera, D. G. *BBA- Bioenergetics* **2004**, *1655*, 13–28.

(11) Doctrow, S. R.; Huffman, K.; Marcus, C. B.; Musleh, W.; Bruce, A.; Baudry, M.; Malfroy, B. *Adv. Pharmacol.* **1997**, *38*, 247–269.

(12) Hillard, E.; Vessières, A.; Thouin, L.; Jaouen, G.; Amatore, C. *Angew Chem Int Edit* **2006**, *45*, 285–290.

(13) Reece, S. Y.; Hodgkiss, J. M.; Stubbe, J.; Nocera, D. G. *Phil. Trans. R. Soc. B* **2006**, *361*, 1351–1364.

(14) Reece, S. Y.; Lutterman, D. A.; Seyedsayamdost, M. R.; Stubbe, J.; Nocera, D. G.

*Biochemistry* **2009**, *48*, 5832–5838.

(15) Reece, S. Y.; Seyedsayamdost, M. R.; Stubbe, J.; Nocera, D. G. *J. Am. Chem. Soc.* **2007**, *129*, 8500–8509.

(16) Reece, S. Y.; Seyedsayamdost, M. R.; Stubbe, J.; Nocera, D. G. *J. Am. Chem. Soc.* **2007**, *129*, 13828–13830.

(17) Pizano, A. A.; Lutterman, D. A.; Holder, P. G.; Teets, T. S.; Stubbe, J.; Nocera, D. G. *Proc Natl Acad Sci U S A* **2012**, *109*, 39–43.

(18) Holder, P. G.; Pizano, A. A.; Anderson, B. L.; Stubbe, J.; Nocera, D. G. *J. Am. Chem. Soc.* **2011**, *134*, 1172–1180.

(19) Choe, K. S.; Salama, J. K.; Stenson, K. M.; Blair, E. A.; Witt, M. E.; Cohen, E. E. W.; Haraf, D. J.; Vokes, E. E. *Radiother Oncol* **2010**, *97*, 318–321.

(20) Martínez-Trillos, A.; Gaya, A.; Maffioli, M.; Arellano-Rodrigo, E.; Calvo, X.; Díaz-Beyá, M.; Cervantes, F. *Ann Hematology* **2010**, *89*, 1233–1237.

(21) Mishchenko, E.; Tefferi, A. *Eur J Haematol* **2010**, *85*, 192–199.

(22) Huang, V.; Lu, X.; Jiang, Y.; Wang, J. Y. *BMC Biol* **2009**, *7*, 35.

(23) Davydov, R.; Osborne, R. L.; Kim, S. H.; Dawson, J. H.; Hoffman, B. M. *Biochemistry* **2008**, *47*, 5147–5155.

(24) Li, F.; England, J.; Que, L. *J. Am. Chem. Soc.* **2010**, *132*, 2134–2135.

(25) Edwards, S. J.; Soudackov, A. V.; Hammes-Schiffer, S. *J. Phys. Chem. B* **2010**, *114*, 6653–6660.

(26) Yoon, M.; Song, H.; Håkansson, K.; Marsh, E. N. G. *Biochemistry* **2010**, *49*, 3168–3173.

(27) Marcus, R. A. *J Chem Phys* **1956**, *24*, 966–978.

(28)    Marcus, R. A. *J Chem Phys* **1957**, *26*, 867–871.

(29)    Marcus, R. A.; Sutin, N. *BBA-Bioenergetics* **1985**, *811*, 265–322.

(30)    Marcus, R. A. *J Chem Phys* **1957**, *26*, 872–877.

(31) Hush, N. S. *J Chem Phys* **1958**, *28*, 962–972.

(32)    Hush, N. S. *T Faraday Soc* **1961**, *57*, 557.

(33)    Marcus, R. A. *J. Phys. Chem.* **1986**, *90*, 3460–3465.

(34)    Miller, J. R.; Calcaterra, L. T.; Closs, G. L. *J. Am. Chem. Soc.* **1984**, *106*, 3047–3049.

(35) Cummins, D.; Gray, H. B. *J. Am. Chem. Soc.* **1977**, *99*, 5158–5167.

(36)    Winkler, J. R.; Nocera, D. G.; Yocom, K. M.; Bordignon, E.; Gray, H. B. *J. Am. Chem. Soc.* **1982**, *104*, 5798–5800.

(37) Nocera, D. G.; Winkler, J. R.; Yocom, K. M.; Bordignon, E.; Gray, H. B. *J. Am. Chem. Soc.* **1984**, *106*, 5145–5150.

(38)    Nocek, J. M.; Zhou, J. S.; De Forest, S.; Priyadarshy, S.; Beratan, D. N.; Onuchic, J. N.; Hoffman, B. M. *Chem. Rev.* **1996**, *96*, 2459–2490.

(39)    Tommos, C.; Skalicky, J. J.; Pilloud, D. L.; Wand, A. J.; Dutton, P. L. *Biochemistry* **1999**, *38*, 9495–9507.

(40)    Wasielewski, M. R. *Chem. Rev.* **1992**, *92*, 435–461.

(41) D'Souza, F.; Das, S. K.; Sandanayaka, A. S. D.; Subbaiyan, N. K.; Gollapalli, D. R.; Zandler, M. E.; Wakahara, T.; Ito, O. *Phys. Chem. Chem. Phys.* **2012**, *14*, 2940.

(42)    D'Souza, F.; Smith, P. M.; Zandler, M. E.; McCarty, A. L.; Itou, M.; Araki, Y.; Ito, O. *J. Am. Chem. Soc.* **2004**, *126*, 7898–7907.

(43)    Listorti, A.; O'Regan, B.; Durrant, J. R. *Chem. Mater.* **2011**, *23*, 3381–3399.

(44)   Kuang, D.; Ito, S.; Wenger, B.; Klein, C.; Moser, J.-E.; Humphry-Baker, R.; Zakeeruddin, S. M.; Gratzel, M. *J. Am. Chem. Soc.* **2006**, *128*, 4146–4154.

(45)   Bauer, C.; Boschloo, G.; Mukhtar, E.; Hagfeldt, A. *J. Phys. Chem. B* **2002**, *106*, 12693–12704.

(46)   Ellingson, R. J.; Asbury, J. B.; Ferrere, S.; Ghosh, H. N.; Sprague, J. R.; Lian, T.; Nozik, A. J. *J. Phys. Chem. B* **1998**, *102*, 6455–6458.

(47) Ohkita, H.; Cook, S.; Astuti, Y.; Duffy, W.; Tierney, S.; Zhang, W.; Heeney, M.; McCulloch, I.; Nelson, J.; Bradley, D. D. C.; Durrant, J. R. *J. Am. Chem. Soc.* **2008**, *130*, 3030–3042.

(48)   Grätzel, M. *Inorg. Chem.* **2005**, *44*, 6841–6851.

(49)   Lo, H.-S.; Yip, S.-K.; Wong, K. M.-C.; Zhu, N.; Yam, V. W.-W. *Organometallics* **2006**, *25*, 3537–3540.

(50)   Riis-Johannessen, T.; Schenk, K.; Severin, K. *Inorg. Chem.* **2010**, *49*, 9546–9553.

(51) Takahashi, K.; Sakai, S.; Tezuka, H.; Hiejima, Y.; Katsumura, Y.; Watanabe, M. *J. Phys. Chem. B* **2007**, *111*, 4807–4811.

(52)   Cukier, R. I. *J. Phys. Chem. B* **2002**, *106*, 1746–1757.

(53) Cukier, R. I. *J. Phys. Chem. A* **1999**, *103*, 5989–5995.

(54)   Hammes-Schiffer, S. *Acc. Chem. Res.* **2001**, *34*, 273–281.

(55) Edwards, S. J.; Soudackov, A. V.; Hammes-Schiffer, S. *J. Phys. Chem. A* **2009**, *113*, 2117–2126.

(56)   Hammes-Schiffer, S. *Acc. Chem. Res.* **2005**, *39*, 93–100.

(57) Hammes-Schiffer, S.; Hatcher, E.; Ishikita, H.; Skone, J. H.; Soudackov, A. V. *Coord Chem Rev* **2008**, *252*, 384–394.

(58)    Mayer, J. M. *Annual Review of Physical Chemistry* **2004**, *55*, 363–390.

(59)    Huynh, M. H. V.; Meyer, T. J. *Chem. Rev.* **2007**, *107*, 5004–5064.

(60)    Hammes-Schiffer, S. *Energy Environ. Sci.* **2012**, *5*, 7696–7703.

(61) Warren, J. J.; Mayer, J. M. *PNAS* **2010**, *107*, 5282–5287.

(62)    León, E. I.; Martín, Á.; Pérez-Martín, I.; Quintanal, L. M.; Suárez, E. *Eur J Org Chem* **2012**, *2012*, 3818–3829.

(63)    Manner, V. W.; Lindsay, A. D.; Mader, E. A.; Harvey, J. N.; Mayer, J. M. *Chem Sci* **2012**, *3*, 230.

(64)    MAYER, J. M. *Acc Chem Res* **2011**, *44*, 36–46.

(65)    Tommos, C.; Babcock, G. T. *Acc. Chem. Res.* **1998**, *31*, 18–25.

(66)    Hoganson, C. W.; Babcock, G. T. *Science* **1997**, *277*, 1953–1956.

(67) Turro, C.; Chang, C. K.; Leroi, G. E.; Cukier, R. I.; Nocera, D. G. *J. Am. Chem. Soc.* **1992**, *114*, 4013–4015.

(68)    Berg, J. M. *Acc. Chem. Res.* **1995**, *28*, 14–19.

(69)    Pavletich, N. P.; Pabo, C. O. *Science* **1991**, *252*, 809–817.

(70)    Young, E. R.; Rosenthal, J.; Nocera, D. G. *Chem Sci* **2012**, *3*, 455.

(71) Young, E. R.; Rosenthal, J.; Nocera, D. G. *Chem Comm* **2008**, 2322.

(72) Young, E. R.; Rosenthal, J.; Hodgkiss, J. M.; Nocera, D. G. *J. Am. Chem. Soc.* **2009**, *131*, 7678–7684.

(73) Weinberg, D. R.; Gagliardi, C. J.; Hull, J. F.; Murphy, C. F.; Kent, C. A.; Westlake, B. C.; Paul, A.; Ess, D. H.; McCafferty, D. G.; Meyer, T. J. *Chem. Rev.* **2012**, *112*, 4016–4093.

(74) Zhang, M.-T.; Hammarström, L. *J. Am. Chem. Soc.* **2011**, *133*, 8806–8809.

(75) Hodgkiss, J. M.; Krivokapić, A.; Nocera, D. G. *J. Phys. Chem. B* **2007**, *111*, 8258–

8268.

(76) Hayes, R. T.; Walsh, C. J.; Wasielewski, M. R. *J. Phys. Chem. A* **2004**, *108*, 2375–2381.

(77) Pettersson, K.; Kilså, K.; Mårtensson, J.; Albinsson, B. *J. Am. Chem. Soc.* **2004**, *126*, 6710–6719.

(78)   Nitzan, A. *Chemical Dynamics in Condensed Phases: Relaxation, Transfer, and Reactions in Condensed Molecular Systems*; Oxford University Press, 2006.

(79) Fukuzumi, S. The Porphyrin Handbook; The Academic Press: San Diego CA, 2000; Vol. 8.

(80)   Watanabe, Y. In *The Porphyrin Handbook*; BIochemistry and Binding: Activation of Small Molecules; The Academic Press: San Diego CA, 2000; Vol. 4.

(81) Liang, Y.; Negus, D. K.; Hochstrasser, R. M.; Gunner, M.; Dutton, P. L. *Chem Phys Lett* **1981**, *84*, 236–240.

# Chapter 2

# Synthesis of Iron Hangman Porphyrin Library

## 2.1 Introduction

Enzyme cofactors manage the different transfer lengths for protons and electrons using bidirectional PCET. Protons have to travel over short distances and "hop" across amino acids or along organized water channels while the electrons can travel much longer distances in and out of active sites. In fact, in some transfers the electron does not need to be coupled to the same proton throughout the whole transfer, and, as it moves along the transport chain it can encounter different protons.[1,2] The only requirement for a PCET process is that the thermodynamics and kinetics of the electron transfer depend on the position of a proton at any given time. The ability to use these different pathways for radical transport and catalytic cycles allows enzyme cofactors to have a remarkable amount of control over both the thermodynamics and kinetics of the process.

Therefore, it is of great interest to design model systems that exhibit precise control over the electron and proton transfer coordinates. Even though bidirectional PCET is common in nature, building systems that incorporate separate coordinates for the electron and proton transfer is synthetic challenging. For this task, the Nocera group has developed "hangman porphyrins" (HPX) which separates the proton and the electron in space, allowing for independent control over the transfer distances.[3] The following chapter will address the new PCET design concepts as well as the synthetic methods for the iron HPX donor system and the electron acceptors. Additionally binding studies of the complexes will be discussed.

## 2.2 Development of a modular system to study PCET

Previous systems in the Nocera group have focused on "hangman" or "pacman"

platforms.[4-7] These porphyrins have one of the *meso* positions functionalized with an organic backbone, usually xanthene or dibenzofuran, that allows for the placement of functional groups above the center face of the porphyrin.[3,5] In general, the synthesis of asymmetrically functionalized porphyrin has many steps, and produces an extremely low product yield. Previous experiments using these constructs required not only the functionalization of the *meso* position for the backbone, but also the functionalization of the *meso* position opposite the backbone with the electron donor or acceptor. The synthetic challenge of appending the acceptor itself at the *meso* position of a porphyrin prevented Justin and Alexander from easily changing their system.[7] Therefore, we sought to design new systems that permitted the study of bidirectional PCET, but at the same time allowed for greater flexibility so that many different donors and acceptors could be screened easily. The new system design gets around the covalent attachment of the electron acceptor by axially coordinating it to the metal center (Fe or Zn) of the porphyrin through a nitrogen donating SF linker, such as pyridine (Figure 1.7b). Porphyrins with axial pyridines attached to the metal are well known in the literature,[8,9] as they mimic biological systems such as iron porphyrin bound to histidine in cytochrome *c*.[8] In particular, $Fe^{III}$ porphyrins with axially bound nitrogen donors exhibit large binding constants.[9] Furthermore, by appending the ED/EA to the pyridine, it can communicate electronically with the metal center while improving system modularity.

Experiments to study the interconversion of $Fe^{III}$ to either $Fe^{II}$ or $Fe^{IV}$ are outlined in Figure 1.7b. Our goal to first target an understanding of the conversion of $Fe^{III}$ to $Fe^{IV}$ arises from the prevalence of high valent, reactive, metal oxos in biology.[10] In order to increase the driving force for PCET in our model system, we turned to higher reduction

38

potential acceptors in proximity to the iron center. FeHPX has an extremely short excited state lifetime ($\sim$30 ps)[11] so excitation of the porphyrin to initiate electron transfer will likely prove ineffective. This problem is also circumvented by the axial coordination of the electron acceptor (EA) (or electron donor, ED, for the $Fe^{II}$case) to the Fe porphyrin center. The transient excited state should initiate electron transfer from the FeHPX to the EA. Since proton transfer is coupled to the oxidation of iron center, we can monitor how the hydrogen bond network changes the rate constant for electron transfer. The proton acceptor is positioned by the pendant-hanging group, which can be changed synthetically. The system is extremely modular; the proton and electron acceptors can be modified independently. Additionally, the steric and electronic environment around the metal center can be controlled by systematically varying the *meso* substituents of the porphyrin.

### 2.2.1 Design of HPX platform

The HPX platform as mentioned above spatially separates the proton and the electron transfer pathways allowing for a thorough investigation of the thermodynamics and kinetics of a bidirectional PCET event. In the following sections, the changes that can be made to the proton and electron pathways are discussed in depth. However, there are modifications to the porphryin platform that can be made that will also affect the PCET event. The HPX platform is ideally situated for coordination of *one* electron donor or acceptor, as the hanging group will block one face of the porphyrin from the bulky acceptor. It is known that FeP will preferentially coordinate two nitrogen-donating ligands to the metal center in a cooperative fashion,[8,9,12] so it is advantageous to have one of the faces of the porphyrin blocked. The ability to direct the EA to the opposite side of

the hanging group will, we predict, direct the hydroxyl group into the gap between the hanging group and the porphyrin face, thereby putting it into position to facilitate proton transfer. Additionally, if the PCET event forms Fe(IV)=O, the HPX will release the EA to maintain a structure that is six coordinate. The release of the electron acceptor will prevent fast back electron transfer and allow for a more stable PCET product.

The HPX porphyrins are of $A_3B$ type, in which the "B" group is the hangman platform and the "A" group can be any number of other functional groups. For our purposes, these other meso positions are phenyl based, and in this study are 2,4,6 trimethylphenyl (mesityl) groups, 4 tert-butylphenyl (t-butylphenyl) groups, and 2,3,4,5,6 pentafluorophenyl (pentafluorophenyl) groups. These particular choices for the A-*meso* positions provide an array of steric bulk and electronic effects. Initial studies will utilize the mesityl HPX, as this has been shown to provide enough steric hindrance to prevent the formation of bisiron(III) µ-oxo dimers.[13] The t-butyl phenyl *meso* groups provide a control for less steric bulk with the hangman porphyrin as there is concern that the mesityl group will prevent the coordination of the acceptor to the metal center. There is a crystal structure showing that with the mesityl porphyrin, a hydroxyl group can fit in the gap between the hanging group and the porphyrin face,[14] but the ability to bind the electron acceptor to the other face is unknown with the given steric bulk of the mesityl groups.

## 2.2.2 Design of the proton donor

To further understand the extent of proton and electron coupling we can complete kinetic isotope effect (KIE) studies on the model system. It has been shown that enzyme activation of C–H bonds *via* hydrogen atom transfer results in significant KIEs.[15-17]

Additionally, experiments using colinear systems[18,19] and theoretical predictions of bidirectional systems[20,21] conclude that if PCET kinetics are limited by proton transfer, KIEs will be very large. The Fe–HPX system isolates the PCET event, allowing us the opportunity to directly probe the coupling of electron and proton. The backbones we have chosen allow us to tune the proton transfer distance; we can install either a proton donor or acceptor as the pendant-hanging group. A previously solved crystal structure shows that when an iron–hydroxyl group is positioned on the porphyrin face directly below a carboxylate hanging group, a hydrogen bond network structuring one water molecule is formed.[14] In hydrophobic solvents, this network may mediate the transfer of the proton to the hanging group. If the large isotope effects that have been proposed are a direct result of proton transfer, little to no effect will be seen in the system with a water bridge. However, as the distance the proton has to travel increases, so will the KIE's.[16] By using different backbones, we can tune the proton distance from the metal in 2 Å steps. A thorough study of each distance with isotopic substitution will complement theoretical predictions about the proton transfer component of the PCET reaction, and its effect on KIEs in enzymatic reactions.[15-17]

### 2.2.3 Design of electron acceptor

For the first set of experiments a photoxidant will be used to generate $Fe^{IV}$. Three constraints are imposed on the EA design. First, the electrochemical potential required to oxidize $Fe^{III}$ to $Fe^{IV}$ is 1.2 V vs. SCE,[22] so the electron acceptor must have an excited state reduction potential greater than this. Second, the acceptor must be photoactive and have a sufficiently long excited-state lifetime for electron transfer to occur. Third, in order to

prevent FRET, the emission features of the EA should not overlap with the porphyrin absorption bands.

For our initial studies, we have chosen the aryldiimide family of photooxidants. Pyromellitic diimide (PI), napthlene diimide (NDI), and perylene diimide (PDI) have excited state reduction potentials ranging from 1–2.5 V versus SCE.[23-25] These potentials can be varied by changing the chemical substitution around the phenyl, napthlene, or perylene core, which provides yet another parameter for tuning.[26] Second, the excited state lifetimes of aryldiimides are known to be 1–20 ns, which should be long enough to transfer an electron as part of a PCET event.[27,28] If they are not, a flash-quench reagent can be used to oxidize the EA excited state, and the resulting hole should be preferentially populated by intramolecular electron transfer from the iron center. Third, all three EA's have well-known spectral features. With the ability to extensively and quickly tune the system simply by changing the EA we intend to complete thorough PCET mechanistic studies of the formation of Cpds I and II.

## 2.3   Synthesis of FeHPX

One of the largest challenges associated with the development of bidirectional PCET model systems is the synthesis of systems that separate the proton pathway and the electron pathway in space. The Nocera group has accomplished this using a series of HPX porphyrins. These porphyrins have been used in studies of $O_2$ activation, hydrogen peroxide dismutation, and hydrogen evolution.[4,5,29,30]

### 2.3.1 Synthesis of metal free HPX

Within the past five years, the synthesis of the HPX platform has been simplified

greatly with the use of a microwave reactor. The synthesis of the metal free compound is completed using statistical porphyrin forming method using Lindsey conditions[31,32] and as such, a mixture of porphyrin products is obtained that can be separated by column chromatography. The synthesis of a library of three FeHPX porphyrins with either mesityl, t-butyl, or pentafluorophenyl in the three meso positions was synthesized to conduct the PCET experiments. Additionally, because the reaction is statistical, there is a mixture of other porphyrin platforms, including the symmetrical "A4" porphyrin for each of the meso groups listed above. These are useful as control compounds to understand the "hanging group effect" and, as they are less precious than the asymmetrical HPX porphyrin, are used for initial control studies. The statistical synthesis is as follows and is shown in Scheme 2.1.[32]

The methyl ester xanthene group that will serve as the proton coordinates can be synthesized from a reported procedure in 5 steps with a reasonable yield.[3] In short, a selective monolithiation can be carried out on xanthene dibromide in dry DMF to produce the monoaldehyde xanthene **2**. Using neopentyl glycol and a catalytic amount of benzene sulfonic acid, the aldehyde group can be protected with an acetal to produce **3** in high yields. Then, lithiation followed by exposure to $CO_2$ gas is carried out on the remaining bromide group on the xanthene resulting in **4**, a xanthene with a carboxylic acid group. Reaction of **4** with sulfuric acid in methanol produces the methyl ester aldehyde xanthene **5** in good yield. This product can now be used in the porphyrin forming reaction.

Under mixed aldehyde conditions **5** can be combined in a 1:3 ratio with another aldehyde of choice and excess pyrrole to form the $A_3B$ HPX porphyrin **6**. The other functional groups for the meso positions are shown in Scheme 1. Microwave irradiation

43

## Scheme 2.1: Backbone synthesis and statistical HPX formation[a]
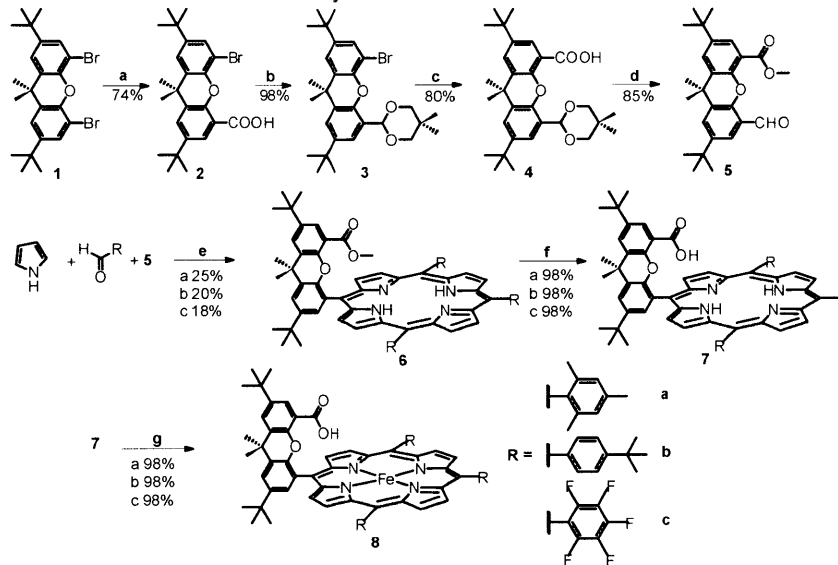


[a](a) PhLi, DMF, THF (b) TsOH, neopentyl glycol, toluene, reflux (c) PhLi, $CO_2$, 2 M HCl, THF (d) (1) TFA, $H_2O$, 24 h rt (2) MeOH, $H_2SO_4$, reflux (e) (1) $BF_3 \cdot OEt_2$, $CHCl_3$, rt, 1 h (2) DDQ, rt 1 h (3) Triethylamine, rt, 10 min (f) (1) 6 N NaOH, THF, 75 °C, microwave irridation 6 h (2) 20% HCl, rt, 12 h (g)15 mol eq $FeCl_2$ 10:3 $CHCl_3$:MeOH 70 °C microwave irridation 6 h. Compounds were characterized by ^{1}H NMR, LD-MS, ESI-MS, elemental analysis, and UV/Vis spectroscopy.

under basic conditions deprotects the methyl ester **6** to produce carboxylic acid **7** in nearly quantitative yields. This step in particular has been optimized with the use of microwave irradiation, as the previous method called for reflux for seven days under nitrogen. Now, with the newly reported synthetic method,[32] deprotection can be completed in a matter of hours. The complexes are then separated using chromatography.

### 2.3.2 Metal insertion

Metallation of the porphyrin **7** is also completed using microwave irradiation and affords **8** in high yield. For the synthesis of FeHPX either iron(II) bromide or iron(II) chloride is used for metallation, and the reaction is run in either 10:3 chloroform:methanol or a small amount of dry dimethylformamide. The reaction using the microwave gives almost quantitative yields and the products can be separated using column chromatography.

44

As mentioned above a library of the FeHPX prophryins was synthesized to understand the electronic and steric effects of varying the non-hanging group meso positions. Therefore FeHPX porphyrins with **a**, **b**, and **c** meso groups were synthesized, along with the corresponding FeA4 symmetric **a**, **b**, and **c** porphyrins for the control studies.

## 2.4 Synthesis of diimide EAs

Manolis Roubelakis completed the synthesis of the three acceptors attached to pyridine for coordination to the metal center. The synthesis of the pyPI and pyNDI can be found in the literature.[33,34] The synthesis of the pyPDI is more complicated, as solubility for this complex is lower than for the other diimide acceptors. Therefore before appending the pyridine ring, some organic chains are appended to the other end of the pyPDI to increase solubility. The synthetic strategy is detailed in section 2.7.

## 2.5 Initial binding studies of FeHPX to EA

Initial studies of the binding strength of pyridyl ligands to $Fe^{II}P$(t-butyl) were conducted. We installed *tert*-butyl groups at the *meso* position of the porphyrin to understand acceptor coordination independent of other effects; they are less sterically hindering than the mesityl group. Fukuzumi and coworkers showed that pyNDI can act as an electron acceptor for ZnTPP (TPP = tetraphenylporphyrin) in benzonitrile.[34] An association constant



**Figure 2.1:** Absorbance (A) and emisson (E) of FeHPX, pyNDI, and pyPDI.

45
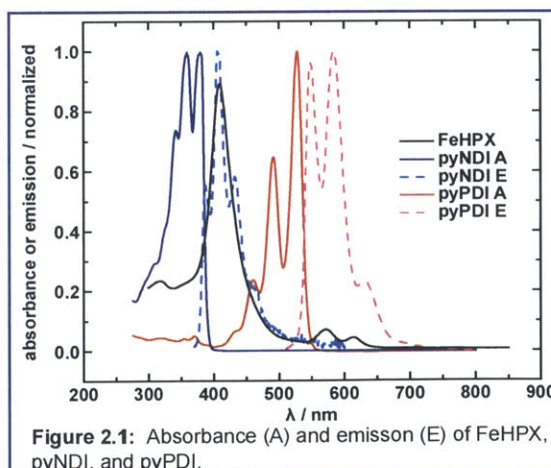
($K_A$) of pyridine to the metal was determined by monitoring specific features in the UV-vis spectrum; the shift in the $\lambda_{max}$ of the Soret and Q bands, and growths and decays that produced isosbestic points.[34] When we repeated these experiments with the Fe$^{II}$P(t-butyl), similar shifts were not observed. The Soret band grew in intensity, which we attribute to the overlap of the absorption of pyNDI and the Soret band of iron porphyrins (Figure 2.1). In a second effort to determine the binding constant between the pyridyl ligand and the FeP, we utilized fluorescence quenching of pyNDI upon addition of FeP. Benesi- Hilderbrand analysis[35] afforded an apparent $K_A$ of 1.8 × 10$^8$ M$^{-1}$ in chloroform, which is several orders of magnitudes higher than the reported value for pyridine and Fe$^{II}$TPP of 10$^3$-10$^4$ M$^{-1}$.[36] Since pyNDI emits at the same wavelength as the Soret band, both inner filter effects and FRET cause a larger quenching effect, and an inaccurate binding constant. The same study was performed with pyPDI–which does not overlap with the porphyrin spectrum in both chloroform and benzonitrile. However, the quenching response of Fe$^{II}$P(t-butyl) was non-linear, which we attribute to the known aggregation behavior of PDI,[37] and a $K_A$ could not be obtained with Benesi-Hilderbrand analysis .

A third way to measure binding to the metal center of the porphyrin is with far infrared (FIR) spectroscopy. Since the coordination complex exists only in solution, solution FIR scans were taken from 700 cm$^{-1}$ to 30 cm$^{-1}$ –a region where metal–atom stretches are well defined. When pyridine and Fe$^{II}$P(t-butyl) were mixed for two hours at room temperature, a new peak was observed at 412 cm$^{-1}$ (Figure 2.2). This correlates well with previously reported stretches of an FeP–imadazole complex.[38] For future studies of the coordination of the acceptor to the porphyrin this method could prove to be very useful for future studies as it gives direct evidence of binding through the pyridine ring to

46
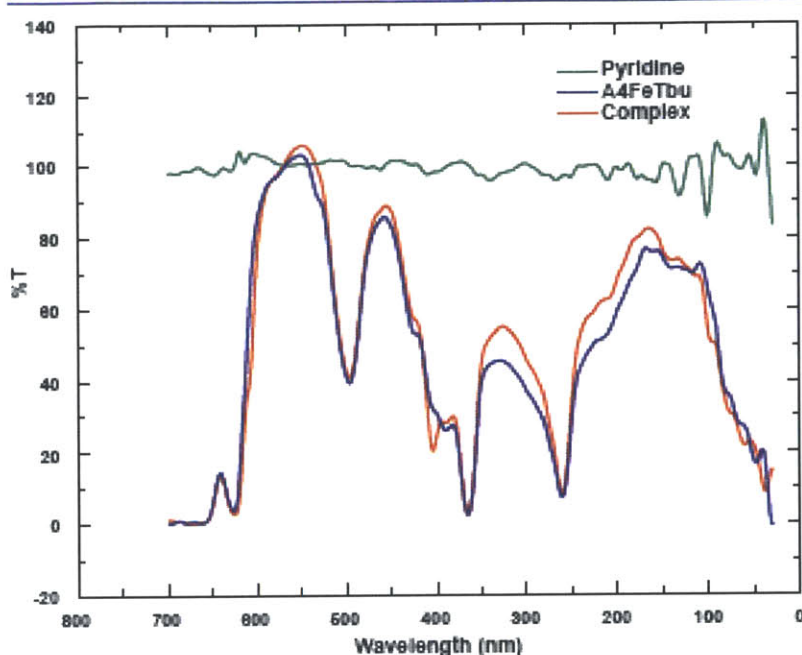
**Figure 2.2**: Far IR spectrum of pyridine, FeA4T-but porphyrin, and complex in $CHCl_3$ (peak at 412nm signifying binding).

the metal center.

## 2.6 Conclusions

As a first step towards building the bidirectional PCET model system to study the interconversion of the oxidation states of heme, we have shown that the HPX porphyrins can be synthesized in a much higher yield than previously reported using microwave assisted synthesis for both the deprotection of the hanging group, and the metal insertion into the free base porphyrin.[32] Three FeHPX systems with different *meso* groups have been synthesized so the steric influences can be studied in depth. In addition, one of the side products of the HPX synthesis is the symmetrical A4 porphyrin, which we can use for preliminary experiments, as it is less precious than the HPX. We can also synthesize the acceptors functionalized with a pyridine ring in relatively high yield from both published and original procedures.

47

After obtaining the donor and the acceptor, we sought to understand the binding mechanism of the acceptors to the FeHPX, as a favorable binding constant is necessary as we plan to excite the acceptor to induce ET. To confirm binding, we initially tried to monitor a shift in the Soret and the Q bands of the porphyrin. However, due to the absorbance overlap of the NDI and the PDI with the Soret, we were unable to get reliable results. It seems like the most reliable way to confirm binding with this system is to take far IR measurements of each sample, as the Fe–N stretch is in a region of the spectra that is separated from the stretches of organic moieties. With the pieces for the PCET scaffold in hand, ultrafast kinetics studies are enabled.

## 2.7 *Synthetic details*

*Chemicals*: All chemicals were purchased from Sigma-Aldrich and used as received unless otherwise noted. Solvents were reagent grade or better and were dried according to standard methods.[39] Silica gel 60 (70–230 and 230–400 mesh, Merck) and Merck 60 F254 silica gel (precoated sheets, 0.2 mm thick) were used for column and analytical thin-layer chromatography, respectively. Spectroscopic experiments employed ACS spectrophotometric grade (≥99.5%) anhydrous toluene, which was used as received. Low chlorin 5,10,15,20-tetraphenyl-21H,23H-porphine zinc was purchased from Sigma-Aldrich.

*Synthesis:* Acceptors BI and NDI were prepared from known procedures.[33,34] For PDI *N*-(4-Pyridyl)-*N'*-(10-nonadecyl)-perylene-3,4,9,10-bis(carboximide) (3), The synthesis of *N*-(10-nonadecyl)-3,4,9,10-perylene-tetracarboxylic-3,4-anhydride-9,10-imide was synthesized using published procedures.[40,41] After, a mixture of the anhydride

(490 mg, 0.74 mmol), 4-aminopyridine (280 mg, 2.98 mmol), and $Zn(OAc)_2$ (83 mg, 0.45 mmol) in 25 ml of quinoline was degassed with $N_2$ and then stirred at 180°C for 5 h under a nitrogen atmosphere. After cooling to room temperature, the solution was treated with 135 mL of aqueous 2N HCl, and the solid was collected by filtration, washed with water and methanol, and condensed under reduced pressure. The compound was purified by column chromatography ($CH_2Cl_2$/MeOH 97/3) to yield a red solid (420 mg, 77%). mp > 350 °C. $^1$H NMR ($CDCl_3$, 400 MHz): $\delta$ 8.85 (dd, $J_1$ = 1.6 Hz, $J_2$ = 4.4 Hz, 2H), 8.50 (m, 4H), 8.28 (m, 4H), 7.41 (dd, $J_1$ = 1.6 Hz, $J_2$ = 4.4 Hz, 2H), 5.13 (m, 1H), 2.22 (m, 2H), 1.90 (m, 2H), 1.25 (m, 28H), 0.82 (t, 6H). $^{13}$C NMR ($CDCl_3$, 100 MHz): $\delta$ 164.00, 162.96, 162.37, 151.08, 142.77, 134.77, 133.30, 131.36, 131.28, 130.56, 129.24, 128.99, 125.96, 125.68, 124.19, 123.95, 123.41, 123.06, 122.65, 122.39, 54.95, 32.28, 31.81, 29.52, 29.51, 29.23, 27.06, 22.59, 14.05. FTIR (ATR, cm$^{-1}$): $\nu$ 2921, 2852, 1698, 1652, 1591, 1575, 1403, 1340, 1253, 1175, 810, 788, 743, 635, 531, 497. MS (ESI) ($m/z$): 734.3962 [M+H$^+$] (Calcd 734.3952). Anal. Calcd for $C_{48}H_{51}N_3O_4$: C, 78.55; H, 7.00; N, 5.73. Found: C, 78.50; H, 6.98; N, 5.89.

## 2.8 References

(1)  Cukier, R. I.; Nocera, D. G. Annu Rev Phys Chem 1998, 49, 337–369.

(2)  Carra, C.; Iordanova, N.; Hammes-Schiffer, S. J. Am. Chem. Soc. 2003, 125, 10429–10436.

(3)  Chang, C. J.; Yeh, C.-Y.; Nocera, D. G. J. Org. Chem. 2002, 67, 1403–1406.

(4)  Rosenthal, J.; Nocera, D. G. Acc. Chem. Res. 2007, 40, 543–553.

(5)  Rosenthal, J.; Chng, L. L.; Fried, S. D.; Nocera, D. G. Chem. Commun. 2007, 2642–

2644.

(6)  Damrauer, N. H.; Hodgkiss, J. M.; Rosenthal, J.; Nocera, D. G. J. Phys. Chem. B 2004, 108, 6315–6321.

(7)  Hodgkiss, J. M.; Krivokapić, A.; Nocera, D. G. J. Phys. Chem. B 2007, 111, 8258–8268.

(8)  Walker, F. A.; Lo, M.-W.; Ree, M. T. J. Am. Chem. Soc. 1976, 98, 5552–5560.

(9)  Kadish, K. M.; Bottomley, L. A. Inorg. Chem. 1980, 19, 832–836.

(10) Weinberg, D. R.; Gagliardi, C. J.; Hull, J. F.; Murphy, C. F.; Kent, C. A.; Westlake, B. C.; Paul, A.; Ess, D. H.; McCafferty, D. G.; Meyer, T. J. Chem. Rev. 2012, 112, 4016–4093.

(11) Liang, Y.; Negus, D. K.; Hochstrasser, R. M.; Gunner, M.; Dutton, P. L. Chem Phys Lett 1981, 84, 236–240.

(12) Cole, S. J.; Curthoys, G. C.; Magnusson, E. A. J. Am. Chem. Soc. 1970, 92, 2991–2996.

(13) Balch, A. L. Inorg. Chim. Acta 1992, 198–200, 297–307.

(14) Chang, C. J.; Chang, M. C. Y.; Damrauer, N. H.; Nocera, D. G. Biochim. Biophys. Acta, Bioenerg. 2004, 1655, 13–28.

(15) Klinman, J. P. Chem Phys Lett 2009, 471, 179–193.

(16) Klinman, J. P. J. Phys. Org. Chem. 2010, 23, 606–612.

(17) Meyer, M. P.; Klinman, J. P. J. Am. Chem. Soc. 2010, 133, 430–439.

(18) Mayer, J. M.; Rhile, I. J. Biochim. Biophys. Acta, Bioenerg. 2004, 1655, 51–58.

(19) Huynh, M. H. V.; Meyer, T. J. PNAS 2004, 101, 13138–13141.

(20)  Johannissen, L. O.; Irebo, T.; Sjödin, M.; Johansson, O.; Hammarström, L. J. Phys. Chem. B 2009, 113, 16214–16225.

(21) Hammes-Schiffer, S. Energy Environ. Sci. 2012, 5, 7696–7703.

(22)   Calderwood, T. S.; Bruice, T. C. Inorg. Chem. 1986, 25, 3722–3724.

(23)   Mataga, N.; Chosrowjan, H.; Taniguchi, S.; Shibata, Y.; Yoshida, N.; Osuka, A.; Kikuzawa, T.; Okada, T. J. Phys. Chem. A 2002, 106, 12191–12201.

(24)   Oelgemöller, M.; Kramer, W. H. J. Photochem. Photobiol., C 2010, 11, 210–244.

(25)   Lee, S. K.; Zu, Y.; Herrmann, A.; Geerts, Y.; Müllen, K.; Bard, A. J. J. Am. Chem. Soc. 1999, 121, 3513–3520.

(26)   Chao, C.-C.; Leung, M.; Su, Y. O.; Chiu, K.-Y.; Lin, T.-H.; Shieh, S.-J.; Lin, S.-C. J. Org. Chem. 2005, 70, 4323–4331.

(27) Ford, W. E.; Kamat, P. V. J. Phys. Chem. 1987, 91, 6373–6380.

(28)   Alp, S.; Erten, Ş.; Karapire, C.; Köz, B.; Doroshenko, A. O.; İçli, S. J. Photochem. Photobiol., A 2000, 135, 103–110.

(29)   Roubelakis, M. M.; Bediako, D. K.; Dogutan, D. K.; Nocera, D. G. Energy Environ. Sci. 2012, 5, 7737–7740.

(30)   Lee, C. H.; Dogutan, D. K.; Nocera, D. G. J. Am. Chem. Soc. 2011, 133, 8775–8777.

(31) Lindsey, J. S.; Schreiman, I. C.; Hsu, H. C.; Kearney, P. C.; Marguerettaz, A. M. J. Org. Chem. 1987, 52, 827–836.

(32)   Dogutan, D. K.; Bediako, D. K.; Teets, T. S.; Schwalbe, M.; Nocera, D. G. Org. Lett. 2010, 12, 1036–1039.

(33)   Harada, K.; Fujitsuka, M.; Sugimoto, A.; Majima, T. J Phys Chem A 2007, 111, 11430–11436.

(34)   Saito, K.; Kashiwagi, Y.; Ohkubo, K.; Fukuzumi, S. J. Porphyrins Phthalocyanines 2006, 10, 1371.

(35) Benesi, H. A.; Hildebrand, J. H. J. Am. Chem. Soc. 1949, 71, 2703–2707.

(36)    Brault, D.; Rougee, M. Biochemistry 1974, 13, 4591–4597.

(37) Tauber, M. J.; Kelley, R. F.; Giaimo, J. M.; Rybtchinski, B.; Wasielewski, M. R. J. Am. Chem. Soc. 2006, 128, 1782–1783.

(38)    Dörr, S.; Schade, U.; Hellwig, P.; Ortolani, M. J. Phys. Chem. B 2007, 111, 14418–14422.

(39)    Armarego, W.; Perrin, D. . Purification of Laboratory Chemicals; 4th ed.; Butterwork-Heinmann: Oxford, 1996.

(40)    Wescott, L. D.; Mattern, D. L. J. Org. Chem. 2003, 68, 10058–10066.

(41) Zhang, Q.; Cirpan, A.; Russell, T. P.; Emrick, T. Macromolecules 2009, 42, 1079–1082.

# Chapter 3

# Defining Important Experimental Parameters Using Nanosecond TA

## 3.1 Introduction

The design of PCET experiments follows from that used for ET experiments, so as to build an understanding of the important parameters that can be controlled in measuring PCET kinetics. The ET rates between porphyrins and coordinated acceptors have been shown for systems utilizing donors such as zinc,[1-3] tin,[4-6] and magnesium[7-9] macrocycles.[10] Therefore, to test the acceptors it is advantageous to work with a system that has been shown to produce CT products in other systems. The FeHPX system of Chapter 2 is precious; hence we sought to establish the most likely conditions for the transient kinetics experiments to produce long-lived electron/hole separation. This will hopefully allow for PT event to the hanging group. We chose to study zinc tetraphenylporphyrin (ZnTPP) as the donor. With this system we can not only determine which acceptor will give us the best chance at charge separation, but can also explore other parameters such as the influence of solvent on both charge separation and binding, the concentration dependence of acceptor and porphyrin, and the signatures that can be expected for the charge transfer events.

## 3.2 Using a Model System for Hangman Porphyrins

As a starting point to understand the basics and limitations of assembly by coordination, we can conduct experiments on a slightly less complicated version of the system we eventually hope to explore, shown in Figure 3.1. Spectroscopic measurements on the target FeHPX system may produce not only complicated traces, but also will be made on a fast timescale (~ps). Therefore, in order to have the best possible chance producing a PCET event, we can optimize some experimental parameters using ZnTPP instead of the FeHPX. Use of ZnTPP allows for measurements of each of the acceptor

systems with a closed-shell d10 porphyrin, instead of the open shell Fe(III) porphyrin. Fe(III) porphyrins are known to have very short excited state lifetimes due to the excited electrons quenching into the partially filled d shell.[11,12] When the d shell is full, as it is in the case of zinc porphyrins, the CT lifetimes are much longer (ns-µs) because there is no chance of self-quenching.[13] Therefore the less complicated experiment of exciting the porphyrin as opposed to the bound acceptor can be performed. Using this system, we can compare the three acceptors that have been synthesized and determine which one is most likely to induce a PCET event in the FeHPX system. Additionally, we can survey different solvents and the effect that changing solvents has on CT rates and the spectral signatures of the radical cation of the porphyrin system and the radical anion of the acceptor. Additionally, we can run the system both with excitation of the porphyrin and excitation of the acceptor, which is necessary to do for the FeHPX experiments.

### 3.2.1 Understanding Limitations Using Zn Porphyrin

As previously mentioned, the ZnTPP porphyrin is closed-shell, which will make ET experiments exponentially less complicated than if the donor were to be a porphyrin that has open d orbitals to quench the excited electron. However, it would be naïve to think that the experiments will directly correspond to the results that will be obtained from the FeHPX system. These experiments are simply to understand the experimental parameters and optimize the system to the best of our abilities, before performing the measurements on a system with a shorter excited state lifetime. Additionally, there are potentially spectroscopic limitations with pyPDI and ZnTPP, as the spectral overlap between the two species is large, which might make selective excitation of the donor

difficult. PyNDI does not have the same degree of overlap with the donor, especially if we selectively excite the Q-bands of the porphyrin, and pyPI does not have any absorption overlap with ZnTPP, and should therefore result in very clean excitation of the donor. The absorption and emission of ZnTPP with each acceptor is shown in Figure 3.2.

## 3.3  NS TA in a Polar Solvent

As a first attempt at CT with the coordinated systems, we tried to repeat the experiments that Fukuzumi et al, performed with the ZnTPP-NDI system in benzonitrile, a fairly polar solvent.[1] It is known that polar solvents will *stabilize* a CS state between a donor and acceptor, but will inhibit coordination of the porphyrin to the acceptor.
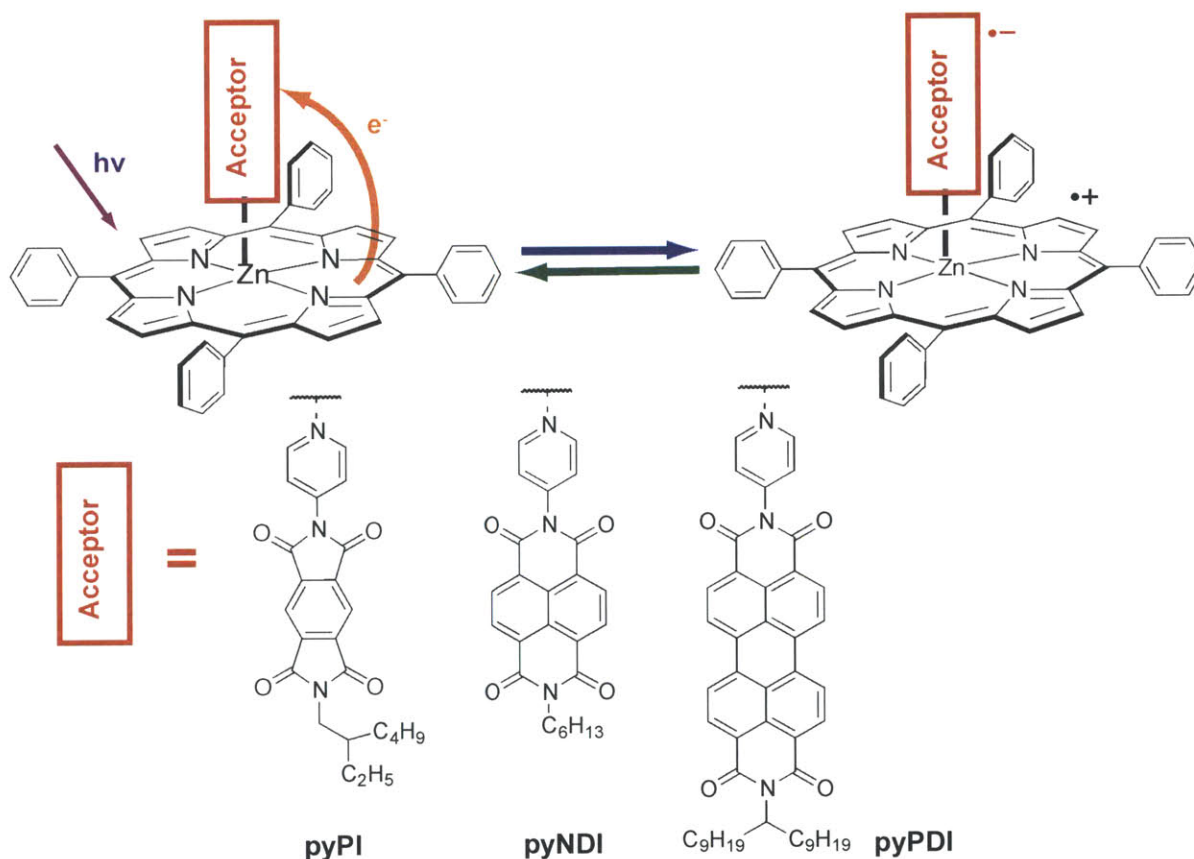


**Figure 3.1:** ZnTPP--Acceptor system to be studied as a "model" system for the FeHPX PCET system. Upon excitation of the ZnTPP with one of the acceptors listed below, an ET event will be induced that can be monitored by TA.

Alternatively, a less polar solvent (like 2-methyl-THF as has been popular for previous ultrafast studies in our lab) can be used to promote binding between the acceptor and the porphyrin, but will *destabilize* the CS state, and produce faster CT.[14,15] For the FeHPX systems, the longer the CS state, the better, especially if the PCET rate is limited by the rate of PT. In that case, the ability to keep the electron and hole separated for as long as possible is extremely advantageous, even more so if there is a chance it will quench into open d orbitals. Therefore, we began the TA experiments with an extremely polar solvent and an extremely large excess of acceptor to ensure that most of the porphyrin is bound. When we try to run experiments with excitation of the acceptor, the concentration of the acceptor must be carefully controlled and therefore the binding will be much lower as there should be little excess. At that point it might be advantageous to switch to a solvent that is less polar to promote binding. Repeating Fukuzumi's experiment first will ensure that our system is working properly, and we can detect the signals of CT.
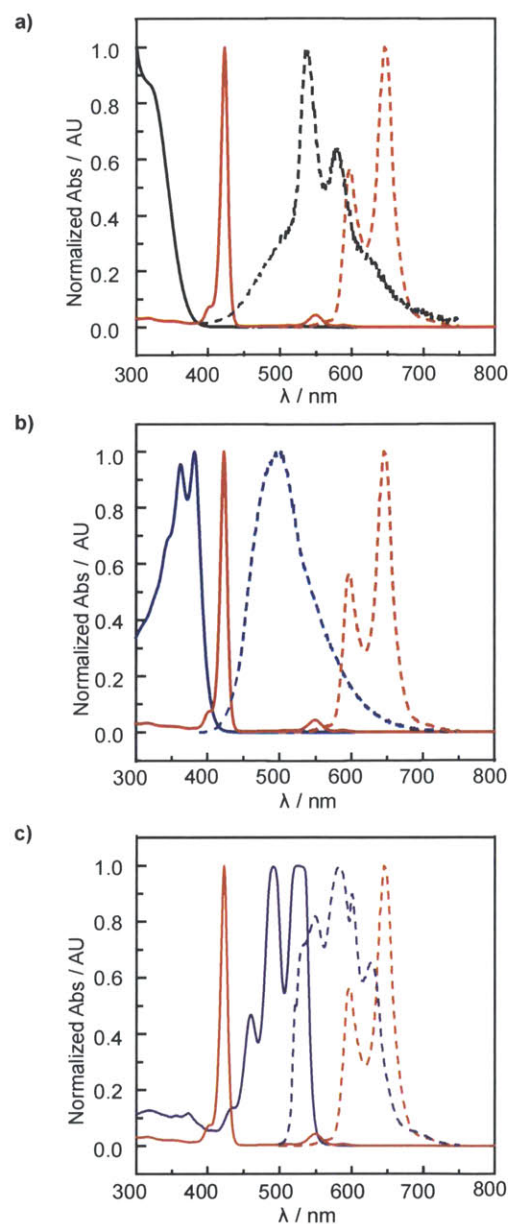


**Figure 3.2:** Steady state Abs (line) and Em (dotted) of ZnTPP (red) and a) pyPI (black), b) pyNDI (blue), and c) pyPDI (purple)

58

### 3.3.1 NS TA

The nanosecond TA setup in the Nocera lab, shown in Scheme 3.1 is a home built system utilizing the third harmonic (355nm) of a Spectra–Physics Quanta–Ray Nd:YAG laser system that produces 300 mJ, 10 ns, 355 nm pulses at 10 Hz. The 355nm output is passed through a (name of MOPO) and is used to pump an OPO that can be tuned over the range of 200–2500 nm to generate the 422nm wavelength used for the pump in the measurements. The probe white light is produced by the output of a 75W Xe arc lamp (Photon Technologies Incorporated). The timed delays were created with delay generators (Stanford Research Systems) and Uniblitz electronic shutters for the pump and the probe (Vincent Associates) were used to control the on/off sequence. The pump and the white light beams are focused and overlap at a 15° angle on the sample, which is contained in a 1cm pathlength quartz cuvette (Starna).

The residual light is passed through a 0.4mm slit into a Triax 320 spectrometer. The signal light is dispersed by a 300 x 500 blazed grating and, for the full spectrum recorded by a gated CCD camera (Andor Technology 1024 x 256 pixels) whose delay and exposure was timed from the output of the SRS delay generator. To calculate the excited state spectra, a series of four spectra are taken using the on/off state of the pump and the probe: I (pump on/
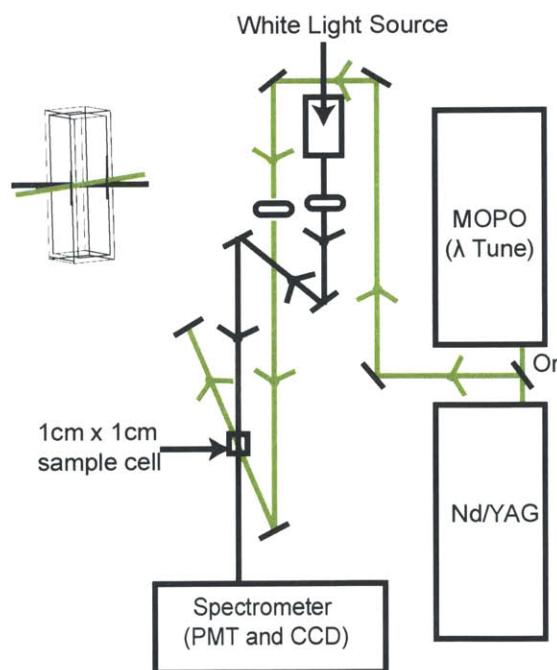


Scheme 3.1: Nanosecond TA setup used for the experiments. The green represents the path of the pump, the black the path of the probe.

probe on), $I_F$ (pump on/probe off), $I_0$ (pump off/probe on), and $I_B$ (pump off/probe off). The background of any light entering the box is accounted for by $I_B$ and the fluorescence is accounted for with $I_F$ spectra. The $\Delta OD$ of the TA is calculated using the following equation:

$$\Delta OD = -\log \frac{I - I_P}{I_0 - I_B}$$

(Eq 3.1)

For single wavelength kinetics, the beam is dispersed using the same grating and passed into the detector through a 0.4mm slit and the resulting pulses were recorded with a photomultiplier tube (Hamamatsu 928A) set to 1.00 kV. PMT outputs were collected and averaged with a 1 GHz oscilloscope (LeCroy 9384M) and transmitted to the computer with a GPBI interface. The oscilloscope trigger was a photodiode that picked up backscatter off the cell. For the SWK series, both the pump and the probe shutters were open for the entire length of the experiment.

To ensure that the pump wavelength was not affecting the collection of either the SWK or the full spectra, a 435 nm long pass filter was placed in front of the spectrometer.

### 3.3.2 ZnTPP–pyNDI

The ZnTPP was excited with 422 nm light and a charge separated state was observed at the first time point after excitation. The spectrum of the charge separated state agrees well with the reported appearance of $\lambda_{max}$= 618 nm of ZnTPP$^{\cdot +}$ and $\lambda_{max}$= 480, 608, and 702 nm for pyNDI$^{\cdot -}$ (Figure 3.3a). The feature at 480 nm decays with a rate constant 220 μs, which is consistent with the known value.[1] The system was then run in reverse, exciting one of the pyNDI bands at 355 nm. A charge-separated state was observed at low concentrations of pyNDI (Figure 3.4) with a lifetime of ~150 μs, which is about half of

60

what the CT rate was with ZnTPP excitation. Additional measurements were undertaken at 422 nm varying the solvent to understand solvent dielectric influence on the charge separation. It is known that polar solvents with high dielectric constants stabilize charge separation. However, higher binding constants can be obtained in non-polar solvents with lower dielectric values.[16] Fukuzmi has shown that a 10-fold increase in the $K_A$ of the ZnTPP-pyNDI system can be achieved using benzene ($\varepsilon$=1) instead of benzonitrile ($\varepsilon$=26), but charge separation is only observed in the latter.[1] To optimize both binding events and charge separation, we tested solvents with intermediate dielectric constants, including acetone ($\varepsilon$=17.7) and benzyl alcohol ($\varepsilon$ =13.0). A charge-separated state was observed in both solvents.

### 3.3.3 ZnTPP–pyPDI

The 422 nm excitation experiments were also performed with the ZnTPP‑pyPDI complex. The excited state reduction potential for PDI and NDI are 2.03 and 2.71 V vs. SCE respectively. PDI has dramatically less spectral overlap with the Soret bands of the
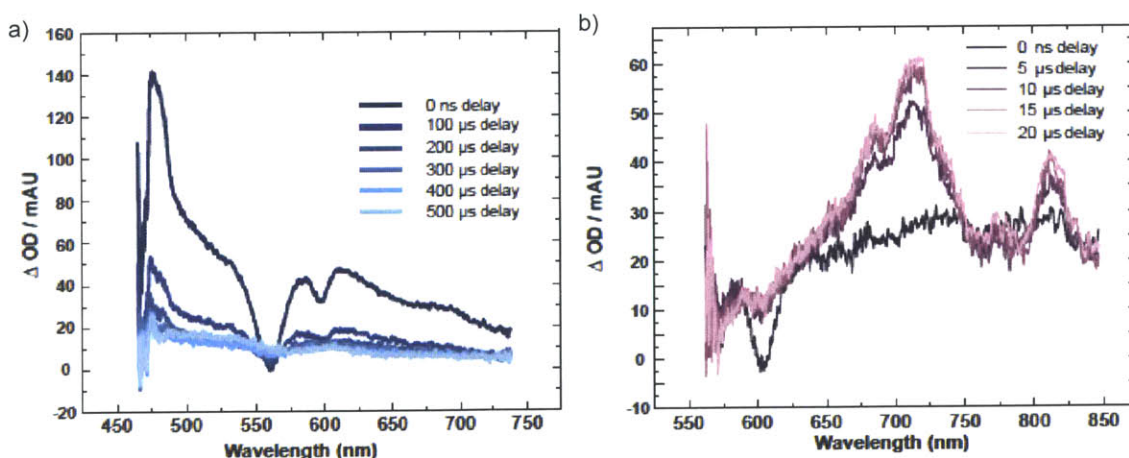


**Figure 3.3:** NS TA with 422 nm excitation for a) ZnTPP--pyNDI showing the decay of the formed CS state at 620 nm and b) ZnTPP--pyPDI showing the formation of the CS state at 710 nm. The SWK showed that for a) the CR rate at 620 nm was ~275 μs and for b) the CS rate was ~4 μs and the CR rate was ~350 μs measured at 710 nm

porphyrin but has an enormous amount of overlap with the Q-bands of the porphyrin (Figure 3.2c). The signatures for PDI$^{\cdot-}$ are also well known.[17] The spectral signatures for pyPDI$^{\cdot-}$ grow in over 20 μs at 710 and 820 nm, (Figure 3.3b) implying that charge separation is much slower in this case. The band at 610 nm is assigned as a Q-band bleach of the porphyrin. Based on our transient absorption kinetic series, the CS state forms in ~5 μs and CR is ~350 μs. Similar to pyNDI we attempted to run the experiment in reverse by exciting the pyPDI at 480 nm, however we were unable to observe clear photoproducts.

### 3.3.4 A Note About Decomposition

To ensure that decomposition was minimal, UV-vis spectra were taken before and after all of the laser experiments. It was found initially that the ZnTPP samples underwent a noticeable amount of decomposition when exposed to UV light, particularly from the white light continuum source. To counteract this, at all times a 400nm long pass filter was placed directly in front of the Xe Arc lamp before the white light passed through the sample. This filter noticeably reduced the amount of decomposition of the sample. Interestingly enough however, no noticeable decomposition was seen when trying to excite the samples at the NDI acceptor (355 nm) with 2 mJ/pulse, suggesting that the decomposition was a result of the intensity of the white light in the deep UV regime.

### 3.4 Conclusions

The experiments conducted with ZnTPP and either pyNDI or pyPDI on a nanosecond timescale give us an enormous amount of insight into considerations for the ultrafast experiment. First, the concentration of the acceptor can be in large excess when we are focusing on excitation of the donor, as the excess acceptor in most cases

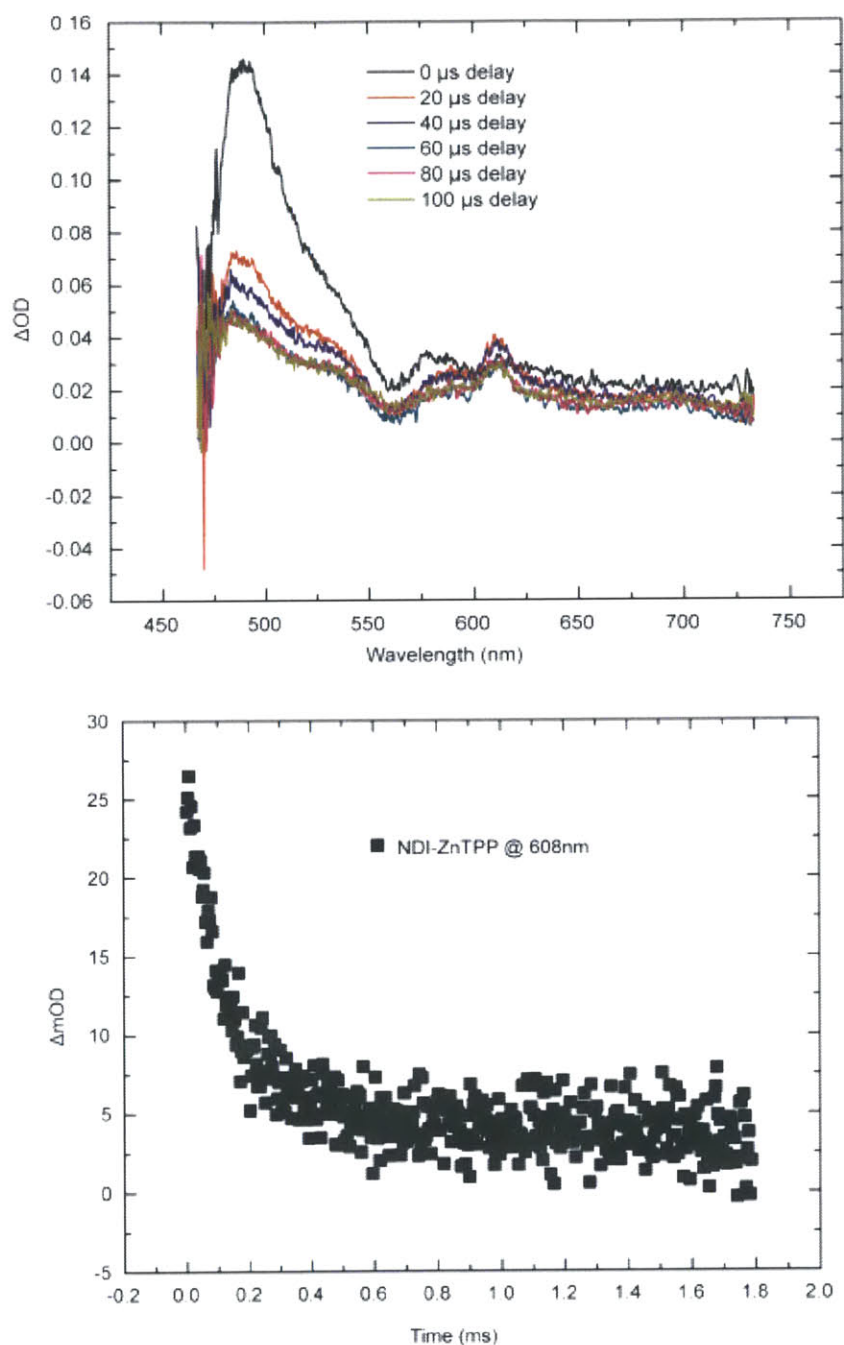**Figure 3.4:** Spectrum of ZnTPP--pyNDI upon excitation of the acceptor at 355 nm. The top spectrum shows the full TA spectrum with the CS signature peak at 620 nm. The lower spectrum is the SWK taken at 608 nm (ZnTPP•+) and has a lifetime of ~150 µs.

will hopefully not obscure the spectrum. In the opposite case however, this acceptor

concentration must be carefully controlled, as we would like to ensure that the signals we

are seeing from the dyad CT are not obscured by the signals from just acceptor. Previously in our group, the ultrafast kinetics can be isolated by probing the sample at the isosbestic point of the excited species.[18] If the acceptors have isosbestic points as the excited state spectrum decays, then we will be able to use this to gain clear insight into the CT kinetics. Additionally it is important to note that the concentration of the pyPDI complex must be carefully considered, as the large extinction coefficient of the pyPDI means we cannot use a large excess of the material and still get signals. Secondly, the decomposition of these compounds must be carefully monitored. The UV output from the white light created some sort of decomposition product with the ZnTPP in PhCN, and when it was cut out, the spectrum was much cleaner. For the ultrafast experiment, the white light is generated by an excess of 800 nm light. We will have to ensure that this excess 800 nm does not degrade the sample in the same way. All of the samples on the ultrafast system will be free of oxygen and water, which will assist in preventing degradation from other sources. Also, experiments on the ultrafast system are required, as the pyPI CT lifetime is too short to observe on the nanosecond timescale. It is useful to know that if the need arises, there are several other solvents that work well with the dyad assembly, and have fairly high dielectric constants. At some point, we will want to optimize the system using a solvent that promotes both binding and charge transfer, so it will be beneficial to choose a solvent with a dielectric constant <26 but >2. We have shown with these experiments that benzyl alcohol ($\varepsilon$=13) will work with the system, and therefore have another option for tuning.

## 3.5 *References*

(1)   Saito, K.; Kashiwagi, Y.; Ohkubo, K.; Fukuzumi, S. J. Porphyrins Phthalocyanines

2006, 10, 1371.

(2)   Harada, K.; Fujitsuka, M.; Sugimoto, A.; Majima, T. J Phys Chem A 2007, 111, 11430–11436.

(3)   Bikram, C. K. C.; Subbaiyan, N. K.; D'Souza, F. J. Phys. Chem. C 2012, 116, 11964–11972.

(4)   Kumar, A.; Giribabu, L.; Maiya, B. Proc. - Indian Acad. Sci., Chem. Sci. 2002, 114, 565–578.

(5)   Giribabu, L.; Rao, T. A.; Maiya, B. G. Inorg. Chem. 1999, 38, 4971–4980.

(6)   Yokoyama, A.; Kojima, T.; Ohkubo, K.; Shiro, M.; Fukuzumi, S. J. Phys. Chem. A 2011, 115, 986–997.

(7)   Ikbal, S. A.; Brahma, S.; Rath, S. P. Inorg. Chem. 2012, 51, 9666–9676.

(8)   D'Souza, F.; El-Khouly, M. E.; Gadde, S.; McCarty, A. L.; Karr, P. A.; Zandler, M. E.; Araki, Y.; Ito, O. J. Phys. Chem. B 2005, 109, 10107–10114.

(9)   Stranius, K.; Jacobs, R.; Maligaspe, E.; Lemmetyinen, H.; Tkachenko, N. V.; Zandler, M. E.; D'Souza, F. J. Porphyrins Phthalocyanines 2010, 14, 948–961.

(10) D'Souza, F.; Ito, O. Coord Chem Rev 2005, 249, 1410–1422.

(11) Liang, Y.; Negus, D. K.; Hochstrasser, R. M.; Gunner, M.; Dutton, P. L. Chem Phys Lett 1981, 84, 236–240.

(12) Guest, C. R.; Straub, K. D.; Hutchinson, J. A.; Rentzepis, P. M. J. Am. Chem. Soc. 1988, 110, 5276–5280.

(13) Scheidt, W. R. In The Porphyrin Handbook: Inorganic, Organometallic, and Coordination; Elsevier, 2003; Vol. 3, pp. 68–80.

(14) Lewis, F. D. Acc. Chem. Res. 1979, 12, 152–158.

(15) O'Driscoll, E.; Simon, J. D.; Peters, K. S. J. Am. Chem. Soc. 1990, 112, 7091–7098.

(16) Holman, M. W.; Yan, P.; Adams, D. M.; Westenhoff, S.; Silva, C. J. Phys. Chem. A 2005, 109, 8548–8552.

(17) Ahrens, M. J.; Kelley, R. F.; Dance, Z. E. X.; Wasielewski, M. R. Phys. Chem. Chem. Phys. 2007, 9, 1469–1478.

(18) Damrauer, N. H.; Hodgkiss, J. M.; Rosenthal, J.; Nocera, D. G. J. Phys. Chem. B 2004, 108, 6315–6321.

# Chapter 4

# Ultrafast Photoinduced Charge Separation and Charge Recombination of Axially Bound Diimide Electron Acceptors to ZnTPP

The work in this chapter is currently in the process of being published:

## 4.1  Introduction

After obtaining rates for charge separation and recombination on the nanosecond system in PhCN for pyNDI and pyPDI, we sought to understand the rates for the acceptor with the largest excited state reduction potential, pyPI. In order to measure this system, ultrafast techniques were used. We sought to measure $k_{CS}$ and $k_{CR}$ for each acceptor coordinated to ZnTPP under the same conditions and so we began studies with ZnTPP–pyPI in benzonitrile (PhCN) using previously developed techniques from the Nocera lab to observe only the CT kinetics.[1] The rate ET rate constants measured can be analyzed within the Marcus framework to understand the relationship between the driving forces and $k_{ET}$. In previous work, the ET rate constants of pyPI coordinated to ZnTPP were reported by excitation of the $S_1$ or $S_2$ states of ZnTPP.[2] In this work, we obtained $k_{ET}$ for each electron acceptor coordinated to ZnTPP upon excitation of ZnTPP $S_1$ only and use the rate constants obtained for a complete Marcus analysis in order to understand driving force relationships to $k_{ET}$ and the regimes of both CS and CR.

## 4.2  Ultrafast TA Spectroscopy System

The ultrafast TA system in the Nocera lab has the ability to measure kinetics up to 6 ns with 1 ps resolution using a mechanical stage. The experimental considerations for ultrafast experiments are inherently more complex than those of the nanosecond system mentioned in Chapter 3. The system is pumped by a subpicosecond LibraHE laser from Coherent Inc., which is described further in Section 4.8.3. The 800 nm ~3.5 W output beam is directed into an OperaSOLO OPA which generates both the wavelengths used to pump the sample, as well as the 800 nm light which is used for the white light probe.

A set-up of the table is shown in Scheme 4.1. The purple line represents the path of the
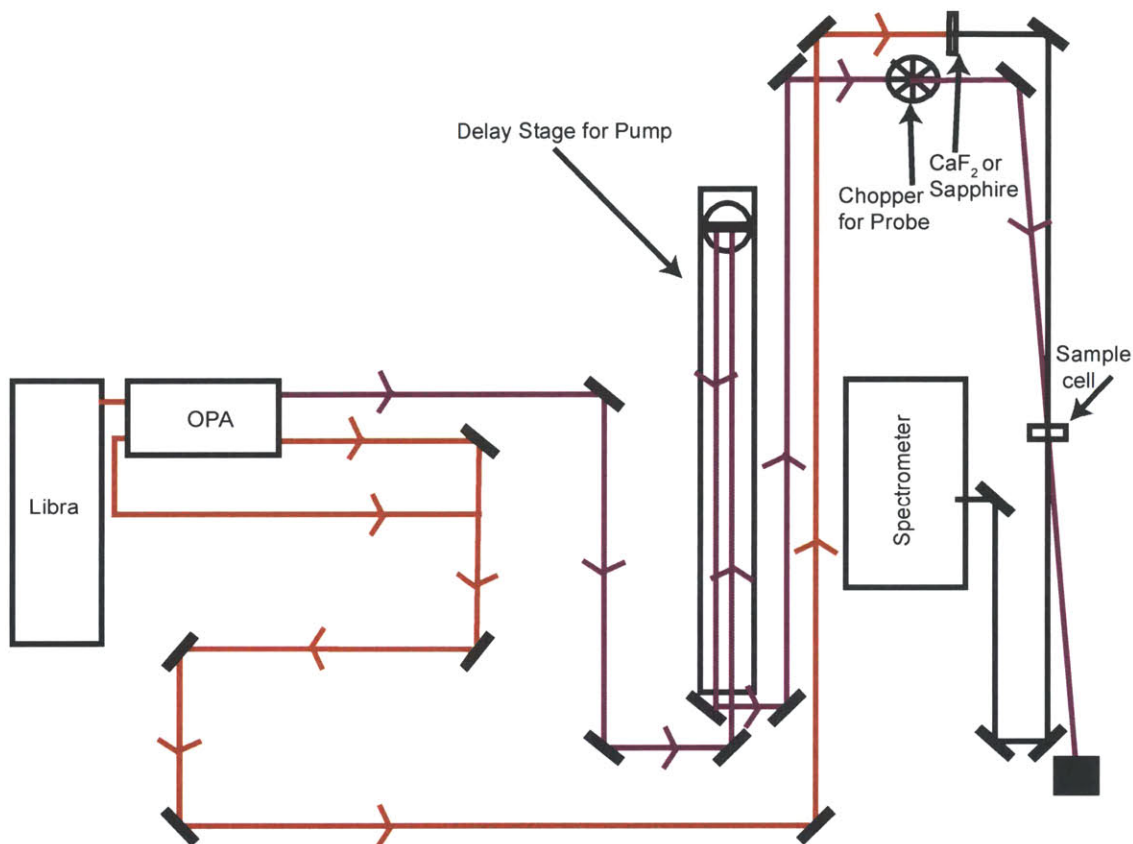


**Scheme 4.1:** Ultrafast TA setup used for experiments.

pump beam and the red/black line represents the path of the probe beam. As shown, the

pump beam is directed onto the mechanical stage for time resolution while the pump

beam is directed around the table to ensure that the two are separated in time such that

there are negative ("zero") timepoints on the stage.

One of the largest challenges of the ultrafast system is the alignment down the

1.7m optical delay stage. The pump and probe beams are about 400μm and must overlap

precisely on the sample. If the pump beam is not exactly aligned down the stage, the data

will not be correct when collected because of drift in the overlap. Therefore, to ensure

that the pump beam is aligned down the stage correctly the beam can be sent a very far

distance around the room, much further than it will travel down the stage, and projected on a white index card. When the stage is moved from end to end, if the laser beam does not move from its original position on the white card, the stage is aligned. Alternatively, a complex with a very long excited state lifetime, such as [tris(bipyridine)ruthenium(II)]$^{2+}$ (Ru(bpy)$_3$)$^{2+}$ in water (which has an excited state lifetime of 630ns[3]) can be used to check the alignment on the stage. This long lifetime results in single wavelength kinetics that look like a step function at all wavelengths, so, if the stage is not aligned the step function will not be flat. This provides an easy way to check alignment and make minor adjustments from day to day. The alignment down the stage will change slightly from day to day and with each unique pump wavelength, as each wavelength will exit the OPA slightly differently.

White light generation for ultrafast TA is also different from methods used in nanosecond TA. Using an 800nm source beam, white light can be generated through a quartz cell, water, or, more commonly, calcium fluoride (CaF$_2$) or sapphire windows.[4] The Nocera lab primarily uses CaF$_2$ windows for better resolution the blue wavelengths, and Sapphire windows for better red resolution. The CaF$_2$ windows must be mounted on a translating stage, so as not to burn holes in the window. This adds an inherent amount of instability to the white light, as the window is constantly moving. Sapphire can give better stability in the white light because it does not need to be translated to prevent burning, but does not produce any probe wavelengths shorter than 450 nm. White light instability can result in untrustworthy data, so the stability of the generated light must be carefully monitored. In the full spectrum mode, self-referencing is possible if the white light beam is split in two before the sample. This way, if there is drift in the white light during the

measurement, it will be cancelled out by the reference.

Additionally all samples must be stirred to prevent local heating and degradation. Porphyrins in particular will undergo thermal lensing, which affects how the laser interacts with the sample and will drastically change the results of the measurement.[5] Therefore, the sample must be stirred directly above or below the pump and probe beam. This ensures that the results obtained are accurate and decomposition is minimized. Absorption spectra were taken of the samples before and after laser experiments to ensure that there was no decomposition of the sample.

## 4.3  Experiments in PhCN

After system setup was completed, a sample of ZnTPP in PhCN was measured on the ultrafast system. In order to successfully isolate and identify the kinetics for the CT process, we use a technique that was developed previously in the Nocera lab.[1] In short, ZnTPP will undergo intersystem crossing (ISC) in about 2 ns for most solvents. When
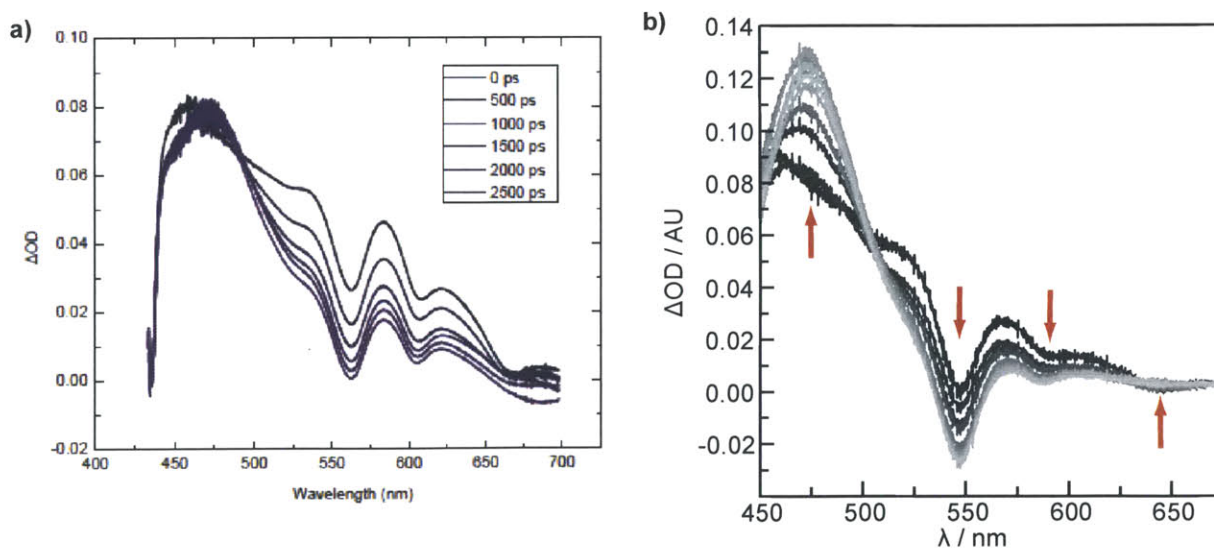


**Figure 4.1:** ZnTPP with 400 nm excitation a)in PhCN from 0 to 2.5 ns (lighter colors are later time points, 500 ps steps) with no clear isosbestic point. b) is ZnTPP in toluene from 0 to 6 ns with clear isosbestic points at ~500 nm and 643 nm.

just the spectra of ZnTPP is measured in 2-methyl- THF, there are clear isosbestic points ~450 nm and ~650 nm that do not change during the conversion from ${}^1$ZnTPP to ${}^3$ZnTPP. These points when measured at 650 nm, the single wavelength kinetics look like a step function, as the spectrum is not changing at that wavelength. Therefore, any exponential signal we obtain at this wavelength when the acceptors are added to the ZnTPP will be from a CT species that is formed upon excitation of the ZnTPP. When ZnTPP was measured in PhCN, however, a clear isosbestic point could not be identified around 650 nm (Figure 4.1a). Due to the importance of this isosbestic point for clear identification of the CT species, the solvent was changed to toluene, which gives a very clear isosbestic point at 643 nm (Figure 4.1b). Therefore, for continuity, all of the acceptors were tested on the ultrafast system in toluene and the single wavelength kinetics were all obtained at 643 nm.

## 4.4 Experiments in Non-Polar Solvent: Toluene

After running the system in PhCN and obtaining inconclusive results for an isosbestic point for ZnTPP, we chose to try to study the system in toluene, as results have been published for a similar study for ZnTPP-pyPI.[2] Toluene is much less polar than PhCN ($\varepsilon$=2.4 for toluene, $\varepsilon$=26 for PhCN) so binding between the acceptors and the porphyrin should be more favorable, but the CS and CR rates will be less stabilized, and therefore faster. Using a sample of ZnTPP in toluene, the isosbestic point was determined to be 643nm (Figure 4.1b); any kinetics obtained at this wavelength therefore can be attributed to the CT process.

## 4.4.1 Binding Studies of ZnTPP to EAs

Solutions of each acceptor in toluene were added to solutions of ZnTPP, and steady state absorption spectroscopy consistently revealed that, upon binding of the electron acceptor to ZnTPP, the $\lambda_{max}$ of the Soret and Q- bands of the ZnTPP shifted by 5 nm and 11 nm, respectively. In addition, isosbestic points between the bound and unbound state were resolved at 425 nm and 555 nm, Figure 4.2 shows the spectrum for the addition of pyPI, the pyNDI looks about the same. These results indicate the generation
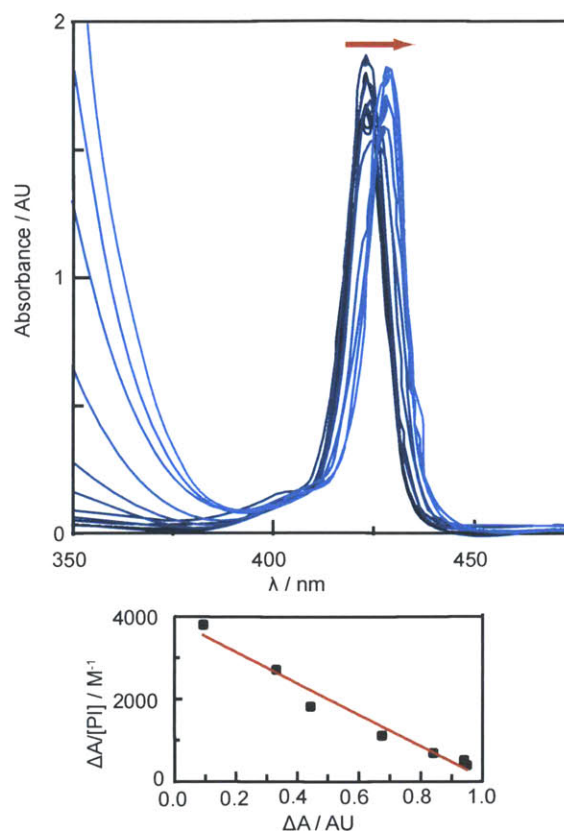


**Figure 4.2:** Absorbance titration of pyPI into a solution of ZnTPP. Isosbestic points are found at 425 nm and 555 nm. The binding constant was calculated as described in the text.

of a pentacoordinated ZnTPP species between each EA and ZnTPP.[6] Binding constants ($K_A$) were determined using the Scatchard method for pyPI (3500 M$^{-1}$) and pyNDI (1300 M$^{-1}$).[7] Titration of the pyPI and pyNDI acceptors into solutions of ZnTPP in toluene also significantly quenched the steady-state florescence the porphyrin, Figure 4.3 shows the result for NDI. This quenching indicates electron and/or energy transfer between the EA and the ZnTPP , which initially indicates that binding has occurred.[8]

In contrast to pyPI and pyNDI, pyPDI binding could not be determined using steady state absorption because the spectral signatures of pyPDI overlap and add into the intensity

of the Soret and Q- bands of the ZnTPP. Instead, the binding constant between pyPDI and ZnTPP was determined by monitoring the spectral shifts in the ¹H NMR of pyPDI as a function of the ratio of ZnTPP to pyPDI, Figure 4.4.[9] The experimental method was as follows. A concentrated stock solution of PDI in $d_8$-toluene was split in half. To one half of a concentrated solution of pyPDI in $d_8$-toluene was added a known amount of ZnTPP in order to
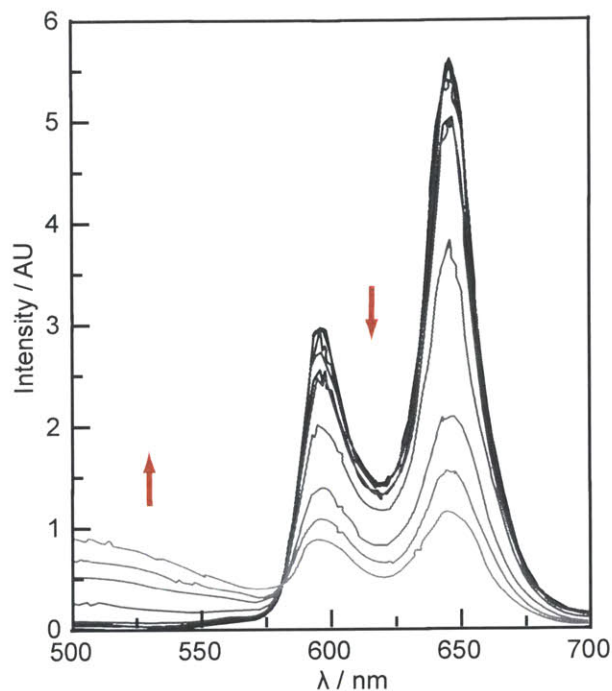


**Figure 4.3:** Fluorescence quenching of ZnTPP upon addition of pyPI.

achieve the highest ZnTPP:pyPDI ratio that ZnTPP solubility permitted. This second solution was titrated into the first, which gradually increased the ZnTPP concentration while maintaining the pyPDI concentration constant. ¹H NMR spectra were recorded after each addition, corresponding to different ZnTPP:pyPDI ratios. The chemical shift of the aromatic hydrogens on PDI changes upon binding ZnTPP. The chemical shift change of these hydrogens was plotted against the concentration of ZnTPP and the data was fit by a non-linear regression of Eq 1[9] in order to derive $K_A$:

$$\delta_{pyPDI} - \delta_{obs} = (\delta_{pyPDI} - \delta_C)\frac{\left([pyPDI]_i + [ZnTPP]_i + \frac{1}{K_a}\right) - \sqrt{\left([pyPDI]_i + [ZnTPP]_i + \frac{1}{K_a}\right)^2 - 4[pyPDI]_i[ZnTPP]_i}}{2[pyPDI]_i}$$

(Eq 4.1)

75

which was determined to be 800 $M^{-1}$. $[pyPDI]_I$ and $[ZnTPP]_I$ are the initial concentrations of the electron acceptor and ZnTPP in solution and $\delta_{pyPDI}$, $\delta_C$, and $\delta_{obs}$ are the chemical shifts of the pyPDI alone, complex, and observed shift respectively.

## 4.4.2 Computational Modeling

Geometry optimized structures of the electron acceptor coordinated to the ZnTPP were obtained using a B3LYP level of convergence with ORCA, to better understand the HOMO–LUMO gap and the center-to-center distance for charge transfer.[10] From the energy levels and the structures visualized in JMol, the HOMO lies on the porphyrin while the LUMO resides entirely on the acceptor,



**Figure 4.4:** Determination of the binding constant for ZnTPP and pyPDI using NMR. The calculation for the binding constant is described in the text.

Figure 4.5 shows the results obtained for ZnTPP-pyPI, the pyNDI and pyPDI are similar. The pyridine, therefore, acts as a spacer molecule and likely does not contribute to the LUMO. From these calculations the center-to-center distance of the donor and acceptors

76

can be measured, and the values are reported in Table 4.1. The calculations agree with results obtained in similar studies.[2]

### 4.4.3 Electrochemistry

In order to calculate the electron-transfer driving force ($\Delta G_{ET}$) in each dyad, the oxidation potentials ($E_{red}$)



**Figure 4.5:** HOMO (left) and LUMO (right) of the ZnTPP--pyNDI complex. Both pyPI and pyPDI exhibited the same structure for the HOMO and the LUMO.

of each electron acceptor and the reduction potential ($E_{ox}$) of ZnTPP were measured by cyclic voltammetry. These potentials are summarized in Table 4.1. The driving force of the charge separation ($\Delta G_{CS}$) and charge recombination ($\Delta G_{CR}$) can be estimated by using the following equations:[11]

$$-\Delta G_{CS} = E_{red} - E_{ox} + E_{00} + \Delta G_{S} \qquad \text{(Eq 4.2)}$$

and

$$-\Delta G_{CR} = E_{00} + \Delta G_{S} \qquad \text{(Eq 4.3)}$$

where

$$\Delta G_S = e^2 \left( \frac{1}{2r_D} + \frac{1}{2r_A} \right) \left( \frac{1}{\varepsilon_m} - \frac{1}{\varepsilon_s} \right) - \frac{e^2}{e_m r} \qquad \text{(Eq 4.4)}.$$

The values of $E_{red}$ and $E_{ox}$ are the reduction potentials versus Fc/Fc$^+$ for the donor and acceptor, respectively. The singlet excitation energy ($E_{oo}$) was estimated to be 1.9 eV from the fluorescence of the S$_1$ state of ZnTPP. The effective radii of the donor$^{\cdot+}$ ($r_D$) and acceptor$^{\cdot-}$ ($r_A$) are known, Table 4.1.[2,12,13] The center-to-center distances of the donor and acceptor ($r$) were determined by the MO calculations described above and are cited in Table

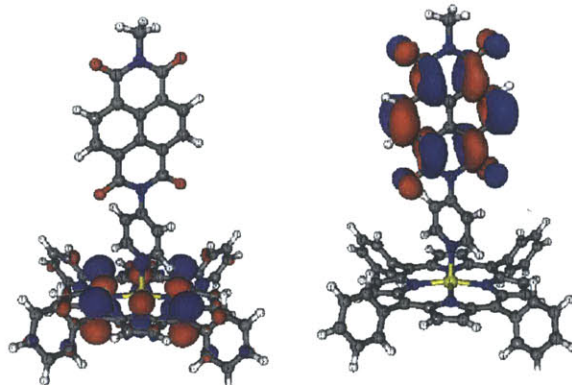|  | $E_{ox}$ (V)[a] | $E_{rd}$ (V)[a] | Radius (Å) | C-C distance (Å) | $-\Delta G_{CS}$ | $-\Delta G_{CR}$ |
|---|---|---|---|---|---|---|
| ZnTPP | 0.318 | -- | 5 | -- | -- | -- |
| PI | -- | -1.22 | 3.5 | 9.88 | 0.71 | 1.18 |
| NDI | -- | -1.02 | 4.0 | 10.02 | 0.91 | 0.99 |
| PDI | -- | -1.00 | 4.7 | 12.2 | 0.93 | 0.97 |

**Table 4.1:** Important properties of the donor and the series of acceptors studied. The redox potentials were measured in Benzonitrile, and the center to center distances of the molecules was determined from the MO calculations. The free energy of CS and CR was calculated using the Marcus Equation described in the text.

4.1. The dielectric constants of the solvent employed during electrochemistry (PhCN) and spectroscopy (toluene) are represented by $\epsilon_m$ and $\epsilon_s$ respectively. It has been shown that Eq 4.3 gives accurate values for $-\Delta G_s$ in polar solvents compared to experimental results. However, in nonpolar solvents such as toluene, the values obtained are much smaller than expected compared to experimental results.[11] As such, using a previously reported modification of Eq 4.3, the values obtained for $-\Delta G_s$ are decreased by 0.35 eV so a value is obtained that is closer to the experimentally obtained results for similar systems, allowing facile calculation of $\Delta G_{CS}$ and $\Delta G_{CR}$.[11]

## 4.5 Ultrafast TA in Toluene

For the spectroscopic experiments, pyPI and pyNDI acceptors were used in a 1000-fold excess and, due to limited solubility, pyPDI was used in 10-fold excess. At these concentrations we calculate >80% of ZnTPP will be ligated to NDI and >90% will be bound to pyPI. Due to the large amount of spectral overlap of the ZnTPP and pyPDI, the concentrations for spectroscopy had to be carefully controlled to ensure that the laser pulse selectively excited the ZnTPP. Therefore, the pyPDI could not be used in extreme excess like the other electron acceptors, resulting in a low percentage of dyad available in

78

the spectroscopic experiments (~10%) and a large amount of unbound electron acceptor and ZnTPP in solution.

### 4.5.1 ZnTPP–pyPI

Upon excitation of the ZnTPP–pyPI complex at 550 nm (ZnTPP Q-band excitation), the $S_1$ state of the porphyrin is generated. This excited state transfers an electron to the acceptor, forming the CS state. The most direct evidence of the formation of the charge-separated state are the kinetics measured at the isosbestic point for ZnTPP. Time-resolved kinetics with $\lambda_{obs}$ = 643 nm show that the CS state is formed with $\tau_{CS}$ = 11 ± 2 ps and it subsequently recombines with $\tau_{CR}$ = 540 ± 30 ps, Figure 4.6. The full spectrum of the ZnTPP–pyPI displays a broad band with $\lambda_{max}$ = 620 nm that corresponds to the formation of the ZnTPP$^{·+}$. We were unable to detect the reported peak for the pyPI$^{·-}$ with $\lambda_{max}$ = 720 nm because our observation is limited to $\lambda$ < 700 nm. As mentioned above, the spectroscopy was performed with a 1000-fold excess of pyPI in the solution to ensure that >90% of the ZnTPP was in a complex with pyPI. The pyPI does not absorb at 550 nm, Figure 3.2, allowing selective excitation of the porphyrin moiety.

### 4.5.2 ZnTPP–pyNDI

The ZnTPP–pyNDI complex was photoexcited with a wavelength of 550 nm to generate a CS state as shown in Figure 4.7. The $\tau_{CS}$ was determined by single wavelength kinetic measurements at $\lambda_{obs}$ = 643 nm to be 11 ± 2 ps. Compared to pyPI, the recombination was slowed such that $\tau_{CR}$ = 810 ± 60 ps. The full spectrum of the dyad again displays a growth of a broad peak with $\lambda$ = 620 nm that corresponds to ZnTPP$^{·+}$ that decays upon CR. It is known that pyNDI$^{·-}$ displays a growth feature with $\lambda_{max}$ = 480 nm, however

79

**Figure 4.6:** ZnTPP--pyPI ultrafast TA data. Sample pumped at 550 nm. a) shows the full spectrum (top, in 10 ps steps, lighter is later time points) and the SWK taken at 643 nm for CS. b) CR full spectrum (100 ps steps, lighter is later in time) and SWK at 643 nm.

this feature cannot be resolved from absorption of the $^3$ZnTPP* at the same wavelength. PyNDI$^{\cdot-}$ is known to have a broad absorption with $\lambda_{max}$ = 605 nm, which in this system overlaps with both the absorption of $^3$ZnTPP* and ZnTPP$^{\cdot+}$.[14]

### 4.5.3 *ZnTPP–pyPDI*

Initially, to avoid excitation of the pyPDI molecule, irradiation was performed at the higher energy Q-band of the porphyrin ($\lambda$ = 605 nm). Surprisingly, the kinetics measured at the isosbestic point exhibited the same properties and lifetime as the kinetics of a solution of only pyPDI excited at the same wavelength. We posit that at the wavelength

80

of excitation a population of free pyPDI is convoluted with the signal of the CS species. This was confirmed by comparing the transient spectra of pyPDI alone, ZnTPP alone, and the ZnTPP–pyPDI complex. In a second attempt at resolution, the excitation was moved to the higher energy side of the ZnTPP Soret band ($\lambda_{ex}$ = 400 nm) in order to selectively photoexcite the ZnTPP. This $\lambda_{ex}$ also resulted in signals corresponding to uncomplexed pyPDI. While the signal is small, the ground state absorbance of pyPDI at $\lambda$ = 400 nm is excited by the laser pulse. Therefore, when excited state spectra of pyPDI alone and ZnTPP alone are overlayed ($\lambda_{ex}$), the result is identical to the excited state spectra of
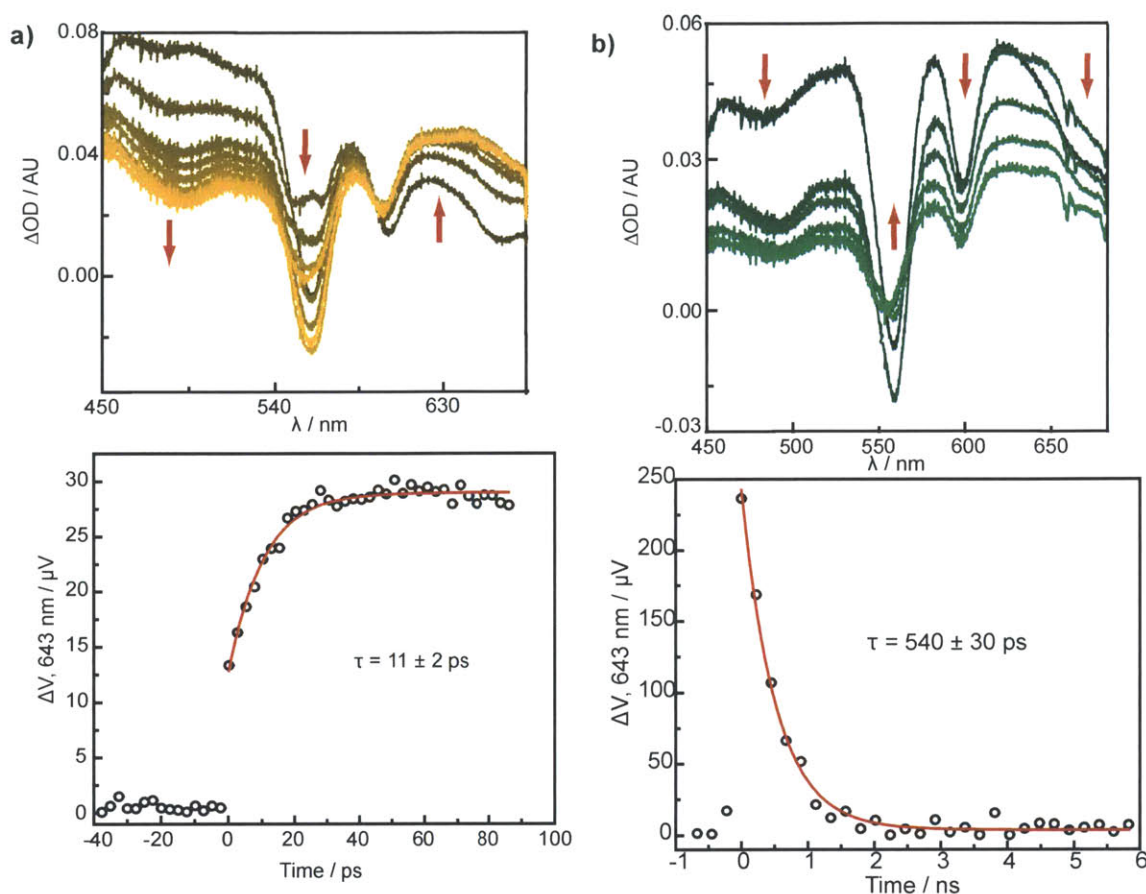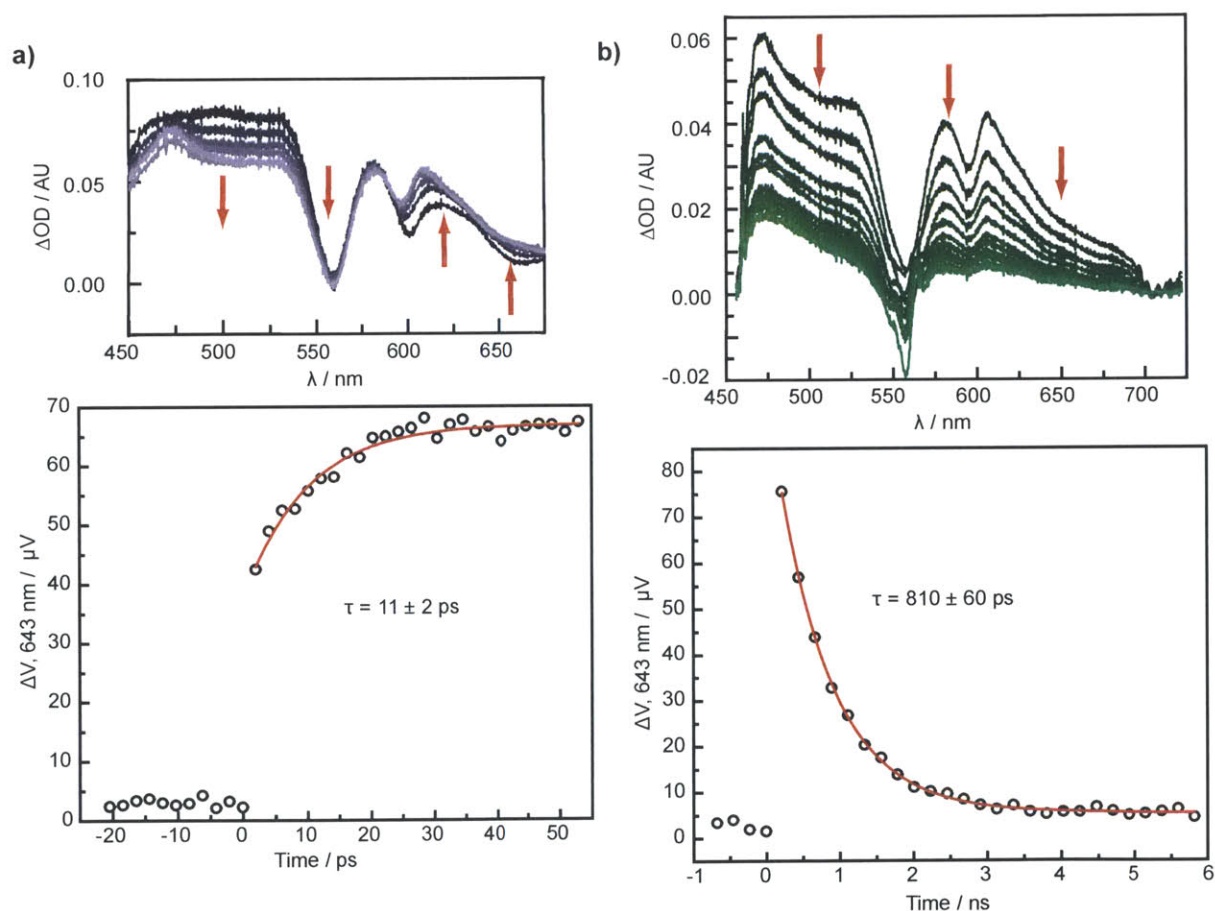


**Figure 4.7:** ZnTPP--pyNDI ultrafast spectra. Sample pumped at 550 nm. a) shows the full spectrum (top, in 10 ps steps, lighter is later time points) and the SWK taken at 643 nm for CS. b) CR full spectrum (250 ps steps, lighter is later in time) and SWK at 643 nm.

ZnTPP–pyPDI mixture. The single wavelength kinetics confirm this finding: at $\lambda_{obs} =$
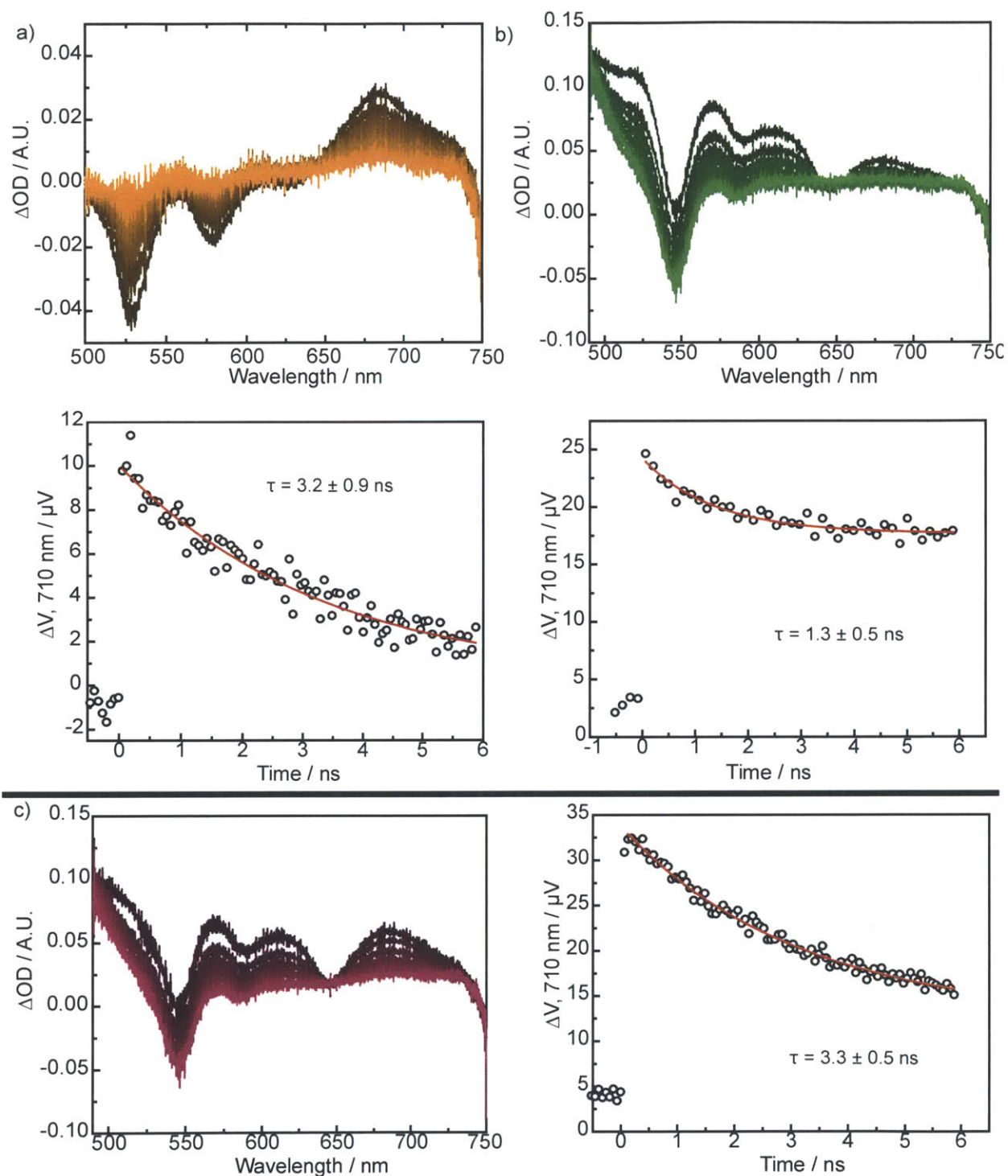


**Figure 4.8:** ZnTPP--pyPDI experiment. Samples pumped at 400nm in each case. a) sample of pyPDI alone, monitoring the SWK at 710 nm. b) Sample of ZnTPP alone, monitoring the SWK at 710 nm. c)Sample of ZnTPP--pyPDI dyad, SWK monitored at 710 nm. In all cases the lighter color is a later time point.

710 nm (corresponding to pyPDI$^{\cdot-}$),[15] the $\tau_{CS}$ for either pyPDI alone or ZnTPP–pyPDI are within the margin of error. The sample of ZnTPP alone also presents a second phase with $\tau = 1.35 \pm 0.5$ ns at $\lambda_{obs} = 710$ nm, which corresponds to the known intersystem crossing (ISC) rate for ZnTPP, Figure 4.8.[16]

Determining ET rates for the ZnTPP–pyPDI dyad was difficult due to the pyPDI absorption in the visible region that overlap with many of the absorption features for the ZnTPP. Therefore, for these spectroscopic measurements unlike those of pyPI and pyNDI, the concentrations of the ZnTPP and the pyPDI were controlled based on amount of spectral overlap determined by the steady state absorbance studies, as there is a high probability for excitation of both free porphyrin and free pyPDI. It should be noted that ZnTPP fluorescence quenching with pyPDI was not shown, as the spectral overlap was such that the amount of quenching could not be spectrally resolved. Additionally, the extinction coefficient of pyPDI is non-trivial, 25,000 M$^{-1}$ cm$^{-1}$ at 490 nm, (ZnTPP= 500,000 M$^{-1}$ cm$^{-1}$ at 422 nm) and covers a broad region of the visible spectrum (~460-530 nm), so the concentration of the acceptor had to be controlled so the white light probe for the spectroscopic experiments could be detected across the wavelengths of interest.

As mentioned above, selective excitation of the ZnTPP in the ZnTPP–pyPDI dyad was difficult to obtain both at the higher energy Q-band and the Soret. Due to a small amount of dyad formed, and therefore a considerable amount of both free ZnTPP and pyPDI, kinetics at both the isosbestic point (643 nm) and the pyPDI$^{\cdot-}$ feature (710 nm) were determined to be composite kinetics of the excited states of ZnTPP and pyPDI alone. Therefore, we were unable to determine rates for this dyad system, and it could not be included in the Marcus analysis.

The absence of charge separation for the ZnTPP-pyPDI sample can partially be attributed to the lack of binding of the acceptor to the porphyrin. Because of the large amount of spectral overlap of ZnTPP and pyPDI and the relatively high extinction coefficients of both species, the concentrations had to be carefully controlled. Therefore as mentioned above the relative amount of binding was small compared to the free species in solution. Additionally the pyPDI electron acceptor has the lowest excited state reduction potential of the different acceptors tested. Finally, the radical cation species of the pyPDI acceptor has peaks at 705 and 950 nm.[15] As stated in the experimental, to generate white light an 800 nm beam is passed through a $CaF_2$ crystal, however there is a portion of 800 nm beam that is not used for generation that passes through the crystal. This light will saturate the CCD detector, so a 800 nm cutoff filter was used. With this filter we were able to detect if there was the formation of a radical anion peak in the 705 nm regime, but no formation or decay kinetics were detected. The radical anion peak at 950 nm cannot be detected by our current set up.

## 4.6 Marcus Analysis of Experimental Results

$k_{ET}$ was calculated from experimental data for both ZnTPP–PI and ZnTPP–NDI, the two complexes that conclusively produce a CS state. Figure 4.9 compares the observed $k_{ET}$ reported in Table 4.2 to ΔG for each dyad reported in Table 4.1. The traditional Marcus

| | ZnTPP-pyPI | ZnTPP-pyNDI | ZnTPP-pyPDI |
|---|---|---|---|
| CS ($10^{10}$ s$^{-1}$) | 9.09±1.6 | 9.09±1.6 | -- |
| CR ($10^9$ s$^{-1}$) | 1.85±0.02 | 1.22±0.08 | -- |

**Table 4.2:** CS and CR rates for the dyads studied in Toluene.

equation,[17]

$$k_{ET} = \frac{2\pi}{h}|H_{AB}|^2 \frac{1}{\sqrt{4\pi\lambda k_B T}} \exp\left[\frac{-(\Delta G + \lambda)^2}{4\lambda k_B T}\right]$$  (Eq 4.5)

can be used to simulate parabolas for the data, where the reorganizational energy ($\lambda$) is defined by two components, the solvent reorganization energy $\lambda_s$ and the internal reorganization energy $\lambda_v$ such that

$$\lambda = \lambda_s + \lambda_v$$  (Eq 4.6)

and in turn, the solvent reorganization energy is defined as[2]

$$\lambda_s = e^2 \left(\frac{1}{2r_D} + \frac{1}{2r_A} - \frac{1}{r}\right)\left(\frac{1}{\varepsilon_\infty} - \frac{1}{\varepsilon_s}\right)$$  (Eq 4.7)

in which $\epsilon_\infty$ is the optical dielectric constant of the solvent in which the spectroscopy was performed, and $\epsilon_s$ is the dielectric constant of the solvent. The calculated $\lambda_s$ for CS systems in toluene (and other nonpolar solvents) are generally much smaller than is experimentally observed because $\epsilon_\infty$ and $\epsilon_s$ are very similar for nonpolar solvents.[11] Therefore, Eq 4.7 gives a poor approximation for the toluene solvent reorganization energy. As has been successful in similar previous work,[11] a $\lambda_s$ = 50 meV was used in our calculations. In contrast, the *internal* reorganization energy is not determined directly, and so the $\lambda$ variable was allowed to vary in the Marcus equation. A reported value from a similar coordination experiment[18] was used as a starting point for this analysis (0.8
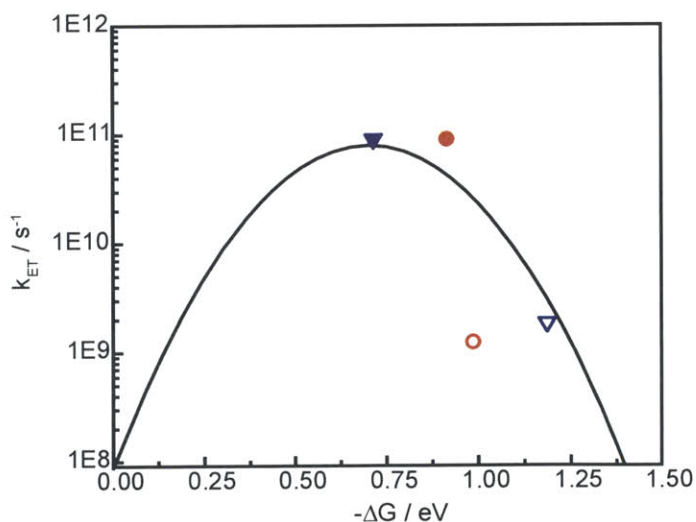


**Figure 4.9:** Experimental results for the CS (closed symbols) and CR (open symbols) rates of ZnTPP--pyPI (red) and ZnTPP--pyNDI (blue) and simulated Marcus Curve for the calculated values of $\Delta G$ as described in the text.

85

eV) where the total reorganization energy for the system was expected to be between 0.1 and 1 eV, so the parameter was allowed to vary between those bounds.[2] The other unknown parameter is the coupling constant between the donor and the acceptor ($H_{AB}$), which can be determined from the overlap of the donor and acceptor wavefunctions. In our calculation this value was also allowed to vary. The starting value was determined in the same fashion from a previous experiment to be 1 meV and then optimized for the data obtained.[11] Using this method, a tentative Marcus parameters can be determined with an $H_{AB}$ coupling constant of 2 meV and a total reorganizational energy of 0.7 eV.

Figure 4.9 displays the calculated Marcus curve based on the rate constants experimentally measured for the ZnTPP–pyPI and ZnTPP–pyNDI dyads. The calculated curve was fit using the experimental results of the donor and acceptor redox potentials, the measured $k_{CS}$ and $k_{CR}$ and the calculated radius of the donor and acceptors, and the calculated center-to-center distance of the HOMO and the LUMO of the coordinated dyad. The curve was calculated using Eq.5. As mentioned above, the coupling constant and the reorganization energies were estimated using values from similar experiments, and were allowed to vary during the fit. Toluene and other non-polar solvents are considered to be close to a "weak coupling limit", that is to say that there is a very small solvent reorganization.[11] Therefore, a correction is made for the weak coupling limit, and a value for the solvent reorganization was used from the literature from a similar experiment (50 meV). Analysis of the best-fit curve to the data suggests that the CS rates lie in the high normal and top Marcus regimes at the maximum of the parabola, promoting very efficient ET. The CR as expected is deep into the inverted regime where the $-\Delta G$ is larger for CR than for CS.[17] From the Marcus plot and the calculated driving force for charge

separation, it is postulated that the pyPI should have a much faster $k_{CS}$ than the pyNDI, however the measured values are virtually the same so the pyPI CS lies further in the top regime of the Marcus curve than that of the pyNDI. For CR we expect that the larger the $-\Delta G$, the slower the recombination rate in the inverted region. From the Marcus plot, we can conclude that the $-\Delta G$ for the pyPI is larger than that of the pyNDI, however CR for the pyNDI is slower. This could be that, because the pyNDI system is more aromatic than the pyPI system, it is better equipped to stabilize the charge across the system. From this we can conclude that both of these acceptors have favorable driving forces to produce a CT product in toluene that lasts for hundreds of picoseconds.

It is known from several other experiments[2,11] that fitting Marcus parabolas to data obtained *in non-polar solvents* results can be problematic. This is attributed to the fact that the estimations for the energy gap law, mainly the contributions of the solvent reorganizational energy and the intramolecular high frequency modes are not well-described in nonpolar solvents. This is described in depth elsewhere.[11,19] Despite this difficulty, the model for our purposes provides satisfactory insight into the regimes of CS and CR and tentative values for coupling (2 meV) and reorganization energy (0.7 eV) for the diimide EAs coordinated to the ZnTPP system.

Ultimately one of the goals of these experiments was to understand in greater detail the considerations that must be taken into account when building coordinated dyad systems, particularly with donors that have much shorter excited state lifetimes than the ZnTPP. Particularly we hoped to understand the efficiency of CT for acceptors with different spectral properties and reduction potentials. For the series of diimide acceptors, CT was observed for the two acceptors (pyPI and pyNDI) with the larger driving force

upon excitation of the ZnTPP. These acceptors were used in a large excess to ensure that the majority of the species in solution was bound dyad. Additionally, toluene was used for the experiments to promote binding. For the pyPDI however, the large amount of spectral overlap between the donor and the acceptor prevented the use of the acceptor in large excess. For the concentrations studied, single excitation of the porphyrin was not attainable, as the unbound portion of the pyPDI was also excited at all wavelengths that were used for the porphyrin, clouding the excited state spectra with pyPDI features. Therefore, we were unable to obtain numbers for CT for the porphyrin and pyPDI due to this spectral congestion and a lack of binding. For future experiments, we can build off the results obtained in the study and start with the acceptor that has the largest driving force for CT. Additionally; the pyPI exhibited a fairly large binding constant in toluene, ($10^4$), so if there is need to extend the lifetime of the CS state, we can use a more polar solvent and still be assured binding with an excess of acceptor. If the pyPI does not produce CT with different donors, the modularity of the system allows changes to be made to the system with little synthetic effort. We have therefore shown an extremely efficient pathway to screening many coordinated donor-acceptor ET systems quickly, as each part can be changed independently for optimization. The diimide complexes used here are a perfect starting point for screening as they display different driving forces and spectral features.

## 4.7  Conclusions

We sought to determine the ET rate constants between three diimide-based acceptors coordinated to ZnTPP, and whether this modular system provides a comprehensive way to screen many donor-acceptor systems for efficient optimization. For these experiments,

88

a series of diimide acceptors attached to a pyridine ring were synthesized to study the difference in CT rates when the reduction potential of the acceptor is varied in the coordinated system. In general, the results follow the expected trend that the acceptors with higher excited state reduction potentials have more efficient charge transfer rate constants than those with lower potentials. The acceptor with the smallest redox potential (pyPDI) did not display any charge transfer signatures that we were able to isolate, which could be due to many different variables, including spectral overlap, inefficient binding, or energy transfer or a small driving force prohibiting ET. The fact that there are so many reasons that the pyPDI may not have worked, led to the conclusion that for future coordinated systems, many of these variables have to be carefully controlled

Unlike covalent systems in which donor and acceptor proximity are ensured, coordinated systems require the biasing of equilibria in solution, and as such can dictate a high concentration of a spectrally dense molecule in solution. This pinpoints an important aspect for biomimetic system design: not only do the reduction potentials have to be well-matched, but binding strength and spectral overlap must also be considered. Particularly for the ZnTPP systems studied here, the coordination to the metal center also ensures that the coupling between the donor and acceptor is strong, whereas when the acceptor is covalently attached to one of the meso positions, the coupling constant is smaller, which could promote energy transfer before electron transfer.[20] This work shows that with a carefully designed system, coordinated dyad models for biology and energy applications are not only feasible but they are extremely modular, such that a range of dyads can be studied with relative ease; the donor and acceptor need only to be mixed in solution before spectroscopic measurements are made. If these molecules had to be synthesized

for covalent attachment, binding is assured for that dyad. If the need arises for a change in the donor or the acceptor, another synthesis must be performed.

## 4.8 Experimental Section

### 4.8.1 Chemicals

Silica gel 60 (70–230 and 230–400 mesh, Merck) and Merck 60 F254 silica get (Precoated sheets, 0.2 mm thick) were used for column and analytical thin-layer chromatography, respectively. All chemicals were purchased from Sigma Aldrich and used as received unless otherwise noted. Solvents were reagent grade or better and were dried according to standard methods.[21] Spectroscopic experiments employed toluene (anhydrous) which was used as received. Low chlorin 5,10,15,20-tetraphenyl-21H,23H-porphine zinc was purchased from Sigma Aldrich. The acceptors were synthesized as described in Chapter 2.

### 4.8.2 Physical Methods

UV-vis measurements were taken at 298K in toluene solutions in quartz cuvettes on a Varian Cary 500 UV-vis-NIR spectrophotometer. Steady state emission spectra were recorded on an automated Photon Technology International (PTI) QM 4 fluorometer equipped with a 150-W Xe arc lamp and a Hamamatsu R928 photomultiplier tube. Excitation light was excluded with appropriate glass filters. Electrochemical measurements were performed on a CH Instruments (Austin, Texas) 760D Electrochemical Workstation using CHI Version 10.03 software. Cyclic voltammetry (CV) experiments were conducted in a nitrogen-filled glovebox at 295 K using a CH Instruments glassy carbon button working electrode (area = 0.071 cm$^2$), BASi Ag/AgNO$_3$ reference electrode, and Pt mesh counter

electrode. The samples had a concentration of 50mM in PhCN with tetrabutylammonium hexafluorophosphate (TBAPF$_6$) as the supporting electrolyte. Scans were taken at either 50mV/sec or 100mV/sec. All CVs were recorded with compensation for solution resistance, and were referenced to the ferrocene/ferrocenium (Fc/Fc$^+$) couple by recording the CVs of the complexes in the presence of a small amount of ferrocene. Appropriate background scans were subtracted from all CVs. Solutions were stirred between acquisition of individual CVs and the working electrode was polished before each measurement.

### 4.8.3 Transient Spectroscopy

All spectroscopic samples were prepared in high vacuum cells consisting of a 2mm pathlength clear fused quartz cell, which was connected to a 10-cm$^3$ solvent reservoir via a graded seal. The two chambers were isolated from the environment and from each other by high-vacuum Teflon valves. A 5µM aliquot of ZnTPP and an aliquot of the electron acceptor both in dry toluene were added to the solvent reservoir. The samples underwent 3 freeze pump thaw cycles under high vacuum (10$^{-5}$ Torr) and were then transferred to the cell and stored under vacuum for all experiments. UV-vis spectrum was taken before and after all spectroscopy to check for decomposition of the sample. All spectroscopy was performed at 298 K. Additionally each acceptor was measured independently at the wavelengths of excitation to ensure a clean excitation of the porphyrin species only.

*Subpicosecond transient spectroscopy:* Picosecond transient spectroscopy was performed on a Coherent Libra HE Ti: Sapphire Amplifier System. The Libra HE incorporates a Coherent Vitesse oscillator that serves as the seed laser for the system. The Vitesse includes the modelocked Ti:Sapphire oscillator cavity pumped by a Coherent Verdi,

a continuous-wave diode-pumped green laser. The Libra system also includes a Coherent Evolution diode pump second harmonic Q-switched laser. The Evolution operates at a single-kHz repetition rate and provides the pump power to the amplifier module. The Libra-HE has an average output power of 3.5 W and a pulse width of 50 fs. The 800 nm output wavelength is directed into a Coherent OPerA SOLO optical parametric amplifier, in which the beam is then split into 2 components, part of the 800 nm light exits the OPA and was focused onto a calcium fluoride ($CaF_2$) substrate to generate the white light probe. A majority of the 800 nm beam is used to generate the range of pump wavelengths in the OPA. Time resolution was achieved by propagating the excitation beam along a computer controlled, 1.70 m long, optical delay line at 1 μm precision (Aerotech ATS 62150). The polarization of pump and probe pulses overlap nearly collinearly in the sample, which was stirred in the axis of beam propagation using a mini-magnetic stirbar. This procedure was implemented to miminize the effects of thermal lensing while maintaining small sample volumes. Both the pump and the probe beam at the sample have a diameter of about 500 μm.

Transient absorption spectra were recorded at discrete times after excitation over the wavelength range 475-800 nm. The spectrum was then resolved in the monochromator (ISA Instruments, TRIAX 320) and recorded on a CCD camera (Princeton Instruments PIXIS). The software to control the system was written in Python. Forward scans only were averaged.

For single wavelength TA kinetics measurements, the pump beam was mechanically chopped at $\omega$ = 500 Hz. The probe beam was spectrally resolved in the monochromator, and a single wavelength was measured on an amplified photodiode. This signal served as

the input for a digital lock-in amplifier (Stanford Research Systems SR830) locked to $\omega$.

The cross correlation of the excitation beam with a single wavelength of the probe beam

has a fwhm = 300 fs for the employed monochromator configuration.

## 4.9 References

(1)   Damrauer, N. H.; Hodgkiss, J. M.; Rosenthal, J.; Nocera, D. G. J. Phys. Chem. B

2004, 108, 6315–6321.

(2)   Harada, K.; Fujitsuka, M.; Sugimoto, A.; Majima, T. J Phys Chem A 2007, 111,

11430–11436.

(3)   Caspar, J. V.; Meyer, T. J. J. Am. Chem. Soc. 1983, 105, 5583–5590.

(4)   Brodeur, A.; Chin, S. L. J. Opt. Soc. Am. B 1999, 16, 637–650.

(5)   Negri, R. M.; Zalts, A.; San Román, E. A.; Aramendía, P. F.; Braslavsky, S. E.

Photochem. Photobiol. 1991, 53, 317–322.

(6)   D'Souza, F.; Ito, O. Coord Chem Rev 2005, 249, 1410–1422.

(7)   Benesi, H. A.; Hildebrand, J. H. J. Am. Chem. Soc. 1949, 71, 2703–2707.

(8)   Lakowicz, J. R. Principles of Fluorescence Spectroscopy; Springer, 2006.

(9)   Wachter, H. N.; Fried, V. J. Chem. Educ. 1974, 51, 798.

(10) Neese, F. ORCA – an ab initio, Density Functional and Semiempirical program

package, Version 2.6. University of Bonn, 2008.

(11) Mataga, N.; Chosrowjan, H.; Taniguchi, S.; Shibata, Y.; Yoshida, N.; Osuka, A.;

Kikuzawa, T.; Okada, T. J. Phys. Chem. A 2002, 106, 12191–12201.

(12) Guo, X.; Gan, Z.; Luo, H.; Araki, Y.; Zhang, D.; Zhu, D.; Ito, O. J. Phys. Chem. A

2003, 107, 9747–9753.

(13) Gómez, R.; Veldman, D.; Blanco, R.; Seoane, C.; Segura, J. L.; Janssen, R. A. J. Macromolecules 2007, 40, 2760–2772.

(14) Saito, K.; Kashiwagi, Y.; Ohkubo, K.; Fukuzumi, S. J. Porphyrins Phthalocyanines 2006, 10, 1371.

(15) Ahrens, M. J.; Kelley, R. F.; Dance, Z. E. X.; Wasielewski, M. R. Phys. Chem. Chem. Phys. 2007, 9, 1469–1478.

(16) Colvin, M. T.; Smeigh, A. L.; Giacobbe, E. M.; Conron, S. M. M.; Ricks, A. B.; Wasielewski, M. R. J. Phys. Chem. A 2011, 115, 7538–7549.

(17) Marcus, R. A.; Sutin, N. Biochim. Biophys. Acta, Bioenerg. 1985, 811, 265–322.

(18) Fujitsuka, M.; Shimakoshi, H.; Hisaeda, Y.; Majima, T. J. Photochem. Photobiol., A 2011, 217, 242–248.

(19) Asahi, T.; Ohkohchi, M.; Matsusaka, R.; Mataga, N.; Zhang, R. P.; Osuka, A.; Maruyama, K. J. Am. Chem. Soc. 1993, 115, 5665–5674.

(20) Hodgkiss, J. M.; Krivokapić, A.; Nocera, D. G. J. Phys. Chem. B 2007, 111, 8258–8268.

(21) Armarego, W.; Perrin, D. . Purification of Laboratory Chemicals; 4th ed.; Butterwork-Heinmann: Oxford, 1996.

# Chapter 5

# Future Directions

## 5.1 Introduction

Efforts to design systems that allow for a thorough study of bidirectional PCET in biology have, until this point, been constructed from covalently bound subunits. We have assembled a bidirectional PCET system from non–covalent, coordinated assemblies of subunits thereby enabling the styudy of fundamental CT properties of several acceptors. These measurements will help us understand the conditions that will provide the best chance for triggering and observing a PCET event in the fully assembled system. We have obtained ET rates for the acceptors upon excitation of the donor (ZnTPP) in both a polar (PhCN) and non-polar (toluene) solvent. The acceptors pyPI and pyNDI were used in a very large excess to ensure that the solution contained mostly bound species. Conversely, or the pyPDI acceptor could not be used in large excess, and correspondingly a CT event was not observed.

These experiments provide important insight into the feasibility of using non–covalent subunits for PCET measurements. As we have found for such an approach, the amount of bound species in the solution is extremely important; if a majority of the species are unbound, it is almost impossible to resolve signal from ET products. The ability to measure the kinetics at the isosbestic point of one of the species can be extremely helpful, if the other free species does not have an absorbance at that wavelength. Therefore, binding must be optimized in the coordinated system either with a large excess of one of the subunits, or by using a non-polar, non-coordinating solvent. To further the point, the ZnTPP-pyPDI assembly did not show signals of CT, however in other experiments with covalently bound the ZnTPP-pyPDI assemblies, resolvable CT bands were observed with TA.[1]

One of the largest differences between the ZnTPP-acceptor system and the FeP system is the excitation used to trigger the CT event. FeP as mentioned before has a very short excited state lifetime due to the electron that quenches into the partially occupied d-orbitals.[2,3] Therefore, we focus our efforts to the excitation of the acceptor. Initial experiments focus on excitation of the acceptor, first using ZnTPP and then the iron analog FeTPP to determine if a CT complex is formed upon excitation.

## 5.2 *Excitation of EAs bound to ZnTPP: Preliminary Results*

Although many experiments have been conducted to measure the charge transfer of diimide acceptors with different donor molecules, there are few experiments that utilize excitation of the acceptor.[4] Initial experiments for excitation of the acceptor focus first on running the system "in reverse" using ZnTPP as the donor, as we have established the spectral signatures we expect for these systems. We begin by testing the two acceptors that produced a CT product in the previous experiment, pyNDI and pyPI.

The $\lambda_{ex}$ for the two acceptors is the same, 340nm, well outside the range of the ZnTPP porphyrin Soret band, ensuring selective excitation of the acceptor Figure 3.2. One of the drawbacks of the excitation of the acceptor is that we can no longer use this compound in large excess to ensure binding. Furthermore, we cannot use a large excess of the ZnTPP in the system, as we want to maintain selective excitation of the acceptors, and at the concentrations used for the experiments in Chapter 3 and 4, there was little to no influence of porphyrin absorbance at the pump wavelength. Initial results with the ZnTPP-pyNDI complex and pyNDI alone pumped at 340 nm and probed at 643 nm showed different kinetics that could not be resolved to obtain a CT rate. Therefore, $\lambda_{probe}$

was shifted to 450 nm, where it is known that NDI·⁻ displays a very large absorbance peak. At 450 nm the single wavelength kinetics are different, but it is not clear if this is due to the influence of absorbance of the excited state porphyrin (which is also seen at this wavelength) or pure ET. Additionally with the large amount of spectral overlap between the NDI and the ZnTPP, it is assumed that there is a large amount of FRET that has to be considered as a quenching mechanism. In an attempt to determine if FRET is a dominant quenching pathway, the emission spectrum after excitation of the acceptor was measured for samples of acceptor alone and dyad: if there is a significant contribution from FRET, we should be able to monitor the formation of the emission of the ZnTPP after excitation of the acceptor. The experiment was conducted using a Streak Camera
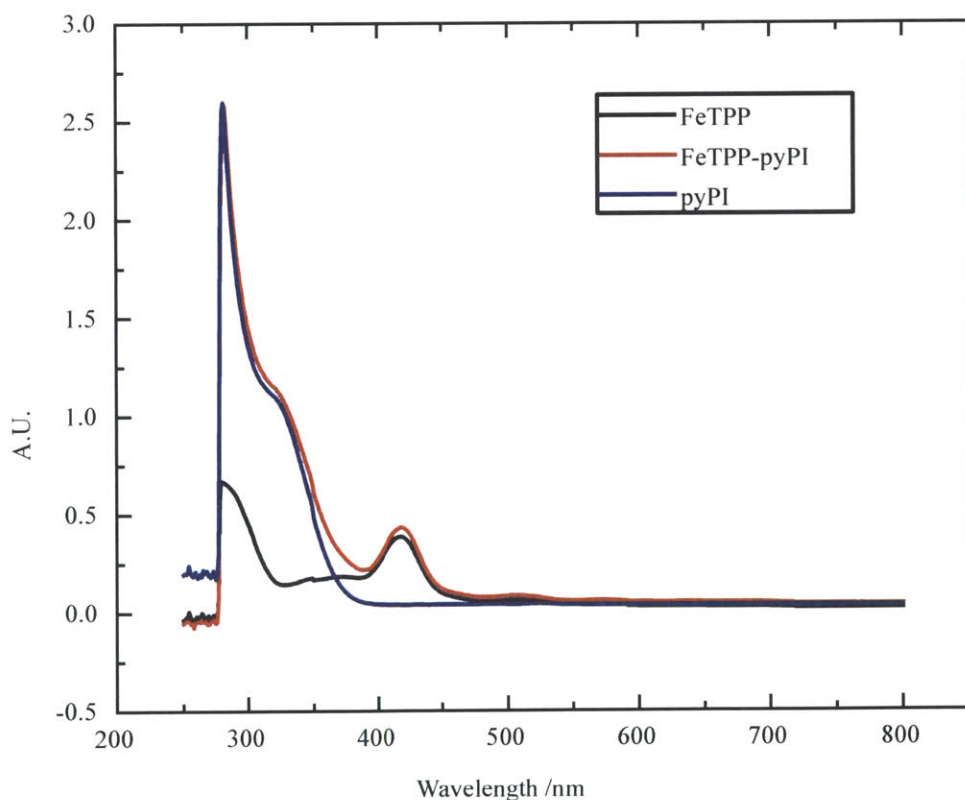


**Figure 5.1:** Steady State absorbance of the FeP, pyPI, and FeP-pyPI samples used for the ultrafast experiments with pump at 340 nm (acceptor excitation)

attached to the ultrafast laser system. The spectrum observed in the regime of expected porphyrin emission shows a difference upon the addition of the donor to the solution of the acceptor. The $\lambda_{ex}$ was 340 nm, affording selective excitation of the acceptor only. To confirm the existence of FRET, steady state emission measurements were undertaken. The steady state emission of the porphyrin is quenched with increasing concentration of the acceptor (increasing the amount bound to the donor), however there is no corresponding increase in the emission of the ZnTPP upon addition of the donor.

## 5.3  Excitation of EAs bound to FeTPP: Preliminary Results

As a "quick and dirty" first attempt at observing CT with an iron based porphyrin, the FeTPP complex was synthesized as described in Section 5.5. The TPP analog was used instead of the FeHPX as the compound is less precious and can be synthesized in larger quantities. The complex was checked for purity by MALDI and assumed to be $Fe^{II}$. The acceptor chosen for initial experiments was PI, as it has the largest driving force for charge separation and spectral features that allow for selective excitation of the acceptor in the dyad. As mentioned above, the PI has a low extinction coefficient, so as compared to the other acceptors it can be used in much larger excess compared to the porphyrin, which will result in a larger amount of bound species. Initial concentrations in toluene were kept the same as the experiment described in Section 5.3 for the ZnTPP system, and $\lambda_{ex}$ is 340 nm.

In contrast to the ZnTPP systems, there is no easily accessible isosbestic point of the acceptors that can be used to obtain unconvoluted kinetics. Therefore initial experiments performed in toluene had a $\lambda_{probe}$ of 710 nm, which is the known location for the radical
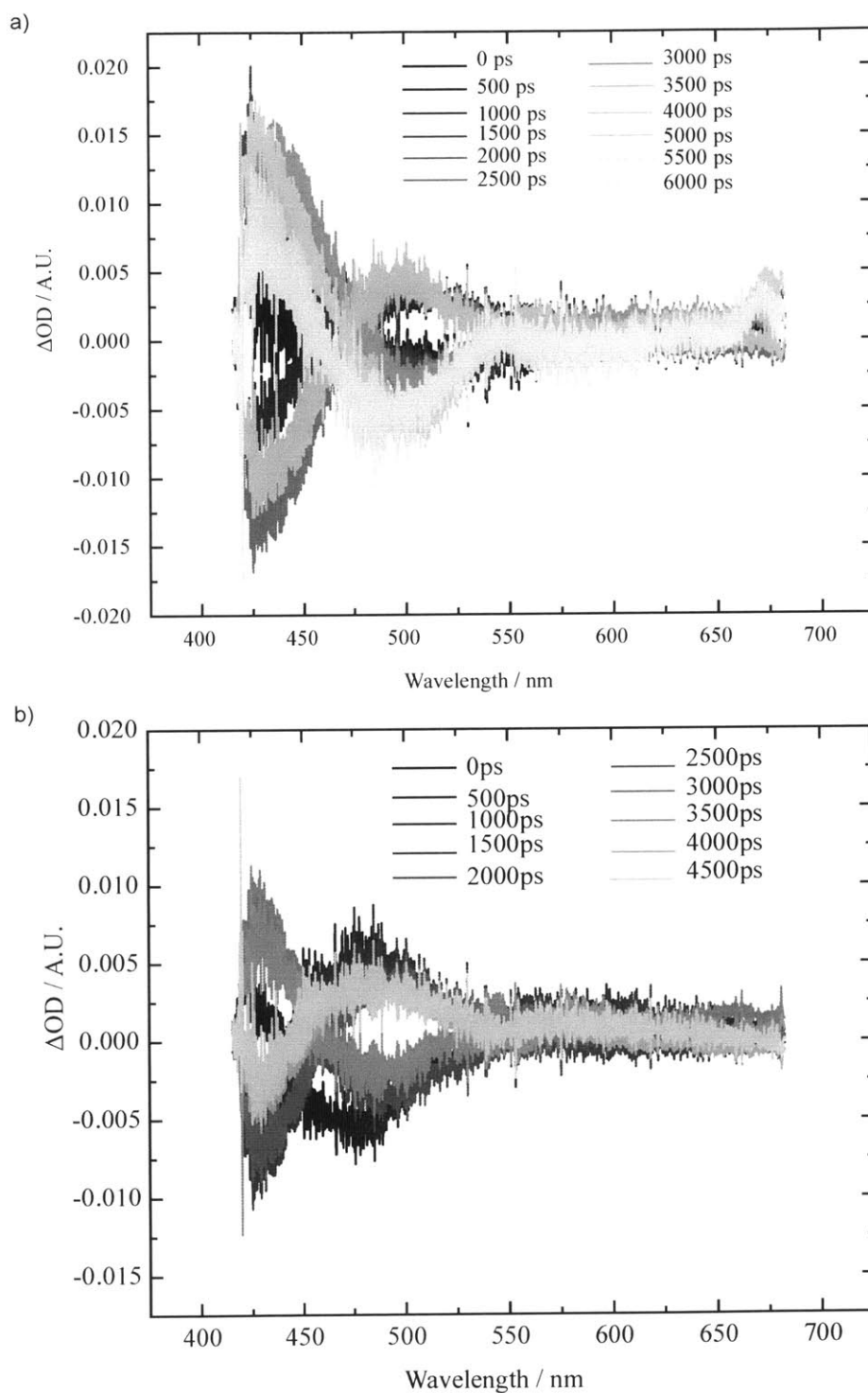
100

a)



b)



**Figure 5.2:** Studies of FeP-pyPI with excitation of the acceptor at a pump wavelength of 340 nm a) is the TA spectra of the pyPI alone, b) is the spectrum of the dyad in toluene. The spectra show no difference, and no CT could be resolved.

anion of pyPI.[5] Additionally, $Fe^{II}$ unlike $Zn^{II}$ will prefer to be six coordinate, and the coordination of the first ligand is cooperative and greatly lowers the energetic barrier for the coordination of a second py ligand. Therefore, there must be an extremely large excess of acceptor to porphyrin to ensure that each porphyrin has at least one acceptor bound. However, the concentration of the acceptor has to be carefully controlled, as the excitation of the acceptor will trigger the ET event. As mentioned above, pyPI is the best candidate for the experiment as it has a small extinction coefficient.

To determine if there is a distinguishable signal for the dyad, samples of pure solvent, (toluene), pyPI alone, porphyrin alone, and porphyrin and acceptor in several different ratios were prepared and subjected to several freeze pump thaw cycles before storage under vacuum in 2mm cells. The samples were each pumped with $\lambda_{ex}$ = 340 nm and the signal is monitored from ~475 – 725 nm. A filter was used to try to exclude 800 nm light from the white light generation, as $\lambda_{probe}$ = 710 nm. Figure 5.1 shows the absorption spectrum of the samples for the acceptor and the porphyrin alone and then the dyad. As can be seen at $\lambda_{ex}$ = 340 nm there should be single excitation of the acceptor species. Figure 5.2 presents the data for a first attempt at CT with the dyad and the spectrum of the acceptor alone as a reference signal. Initially the phasing on the instrument was not set, so although the peak oscillates between positive and negative, no charge separation is detected. The lack of signal from the radical ion however, could be an issue of concentration; there may not be enough of the dyad in solution to clearly see signal from CT. In an effort to increase the amount of dyad bound, we tested different ratios of porphyrin to acceptor; one sample had an excess of porphyrin the other had an excess of acceptor. Again the samples showed no sign of CS, and the spectra looked similar to those shown in Figure 5.2

In a final effort to produce and measure a CT event with the FeP and acceptors, a more polar solvent, PhCN, was used. As mentioned before the higher the polarity of the solvent, the better the solvent helps to stabilize the CS state. However, polar solvents do not promote binding, so the concentration of the assembly will be significantly decreased.

For preliminary tests, a sample of pyPI alone in PhCN and two different samples of dyad, one with a larger excess of pyPI were screened. As shown by the absorption spectrum of the species, there is a slight shift in the Soret band of the porphyrin in the sample with the larger concentration of acceptor, suggesting that more of the porphyrin is bound to the acceptor (Figure 5.3). Upon 340nm excitation, however, no CT was detected and the figure showed no resolvable single wavelength kinetics at any wavelengths.
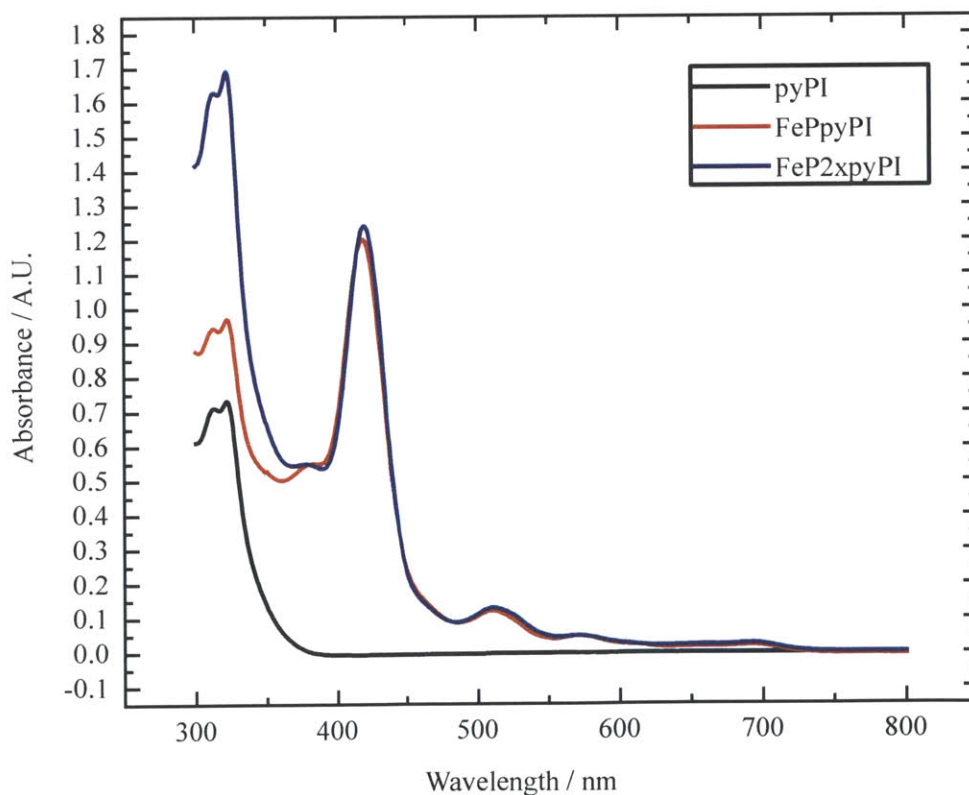


**Figure 5.3:** Steady State absorbance of pyPI, FePpyPI, and FePpyPI with 2x the amount of pyPI in benzonitrile. The shift of the soret band of the FeP suggests that more of the complex is bound with the larger amount of pyPI.

## 5.4 Conclusions and Future Directions

Initial experiments using the acceptors that have been developed with the iron system did not produce a measureable CS state. The lack of CT could be attributed to several factors including but not limited to: a lack of dyad due to cooperative and low binding, energy transfer, or the charge separated state decaying in <1ps. With respect to binding, we can monitor the binding of the acceptor to the porphyrin in the absorption spectrum, and were able to see shifts in the Soret, suggesting binding when an excess of porphyrin or acceptor was added. A careful titration was not completed to compute a precise number for the binding constant, but it is expected to be on the order of $10^4$ $M^{-1}$.

In the future, it would be wise to move away from the use of the diimide acceptors for the FeHPX system. The amount of spectral overlap between the acceptors creates a situation where selective excitation is difficult, and energy transfer will probably be a main quenching pathway of the ET process before PCET takes place. Additionally, the development of a better way to coordinate the acceptor to the metal center must be considered, as the acceptor must be used in excess to ensure that enough of the system is bound and can be detected, potentially out of many other signals from the free compounds in solution. Perhaps in the future, metal complexes that are good electron acceptors can be considered as they have long lifetimes and high excited state redox potentials.

## 5.5 Experimental Section

The A4 FeP was synthesized from 5,10,15,20- tetraphenyl -21H 23H porphyrin (99%) purchased from Sigma Aldrich. The iron source was from iron (II) bromide anhydrous beads -10mesh 99.999% trace metals basis, also purchased from Sigma

Aldrich. A sample of the TPP was added to 4 mL of DMF with 20x equivalents by mole of Fe(II)Br$_2$ and subjected to microwave irradiation for 2 hr. The progress of the reaction was tested by silica TLC in dichloromethane. When the reaction had run to completion, the sample was quickly purified by silica column chromatography using a mixture of 1:10 methanol:dichloromethane. The sample was confirmed to be the FeP A4 product by MALDI and was used for the experiments described above.

## 5.6  References

(1)   Ahrens, M. J.; Kelley, R. F.; Dance, Z. E. X.; Wasielewski, M. R. Phys. Chem. Chem. Phys. 2007, 9, 1469–1478.

(2)   Liang, Y.; Negus, D. K.; Hochstrasser, R. M.; Gunner, M.; Dutton, P. L. Chem Phys Lett 1981, 84, 236–240.

(3)   Guest, C. R.; Straub, K. D.; Hutchinson, J. A.; Rentzepis, P. M. J. Am. Chem. Soc. 1988, 110, 5276–5280.

(4)   Bagui, M.; Dutta, T.; Chakraborty, S.; Melinger, J. S.; Zhong, H.; Keightley, A.; Peng, Z. J. Phys. Chem. A 2011, 115, 1579–1592.

(5)   Harada, K.; Fujitsuka, M.; Sugimoto, A.; Majima, T. J Phys Chem A 2007, 111, 11430–11436.

# Acknowledgements

I would like to thank my thesis advisor Dan Nocera for his unfailing support and guidance, enthusiasm for chemistry, and for giving me the opportunity to work in his lab for 3 years. I learned a lot about not only inorganic chemistry and spectroscopy, but also how to think about and approach interesting problems. Dan's "Make and measure" style of advising was a vital part of my education, giving me both the tools to make what I was interested in studying, and then the systems to study everything about it. His enthusiasm for good science was always infectious, and talking over my research with him was always helpful and inspiring. I'm very thankful for his support.

I also had the good fortune of working with some awesome people in the Nocera lab. Dilek Dogutan Kiper and Matthias Schwalbe were fantastic porphyrin synthetic mentors, and made my first year in the lab very enjoyable (especially Matthias's music choices!). Dilek has served as a mentor in many other capacities, and I'm very thankful for her guidance and support through the years whenever I've needed anything. Team PCET consisted of Patrick Holder, Arturo Pizano, Bryce Anderson and Bon Jun Koo. Pat was another fantastic post doc mentor, listening patiently to my thoughts and concerns and providing lots of guidance and support. Thank GOD he made me use a referencing manager. Talking to Arturo about science is always a pleasure. His vast breadth of knowledge of inorganic spectroscopy was always appreciated and he made conversations, to put it mildly, a blast. Bryce is a fantastic person, and made a lot of this work possible with his enthusiasm of rebuilding all the code for the lasers from scratch and working on the ultrafast system trying to get everything up and running. He was awesome to work with in the lab, and always provided necessary humor for when things didn't work out quite right. Bon Jun has been a wonderful friend and someone I've loved working with. Additionally I'd like to thank Manolis Roumpelakis whose heroic synthetic effort on the acceptors made these experiments possible. Several other people in the lab have been fantastic friends to me over the years, and put up with a lot of my ramblings about life and grad school. Casandra Cox, Andrew Horning, Chris Lemon and Emily McLaurin made work and going to the muddy always an adventure. You guys are fantastic and I wish you all the best in your future endevors.

Outside the Nocera lab several other people deserve special mention. Cliff Kubiak my undergrad advisor was always enthusiastic and helpful whenever I've needed anything over the years. Additionally, the grad student I worked with in his lab, John Goeltz, is still *keeping it real* and has served as a fantastic mentor and source of homebrew. Additionally Michael Funk and Jingnan Lu have been some of the best classmates I could have asked for, and see any occasion as an occasion for wine. Kara Manke has been a fantastic friend and roommate.

Finally I'd like to thank my family, particularly my parents for all of their help, support and understanding, and for believing in me throughout.

106

# Christina Hanson

## EDUCATION:
BS Chemical Physics, June 2008 University of California, San Diego
SM Inorganic Chemistry 2009-2012 Massachusetts Institute of Technology
Concentration: Ultrafast Transient Absorption Spectroscopy of Porphyrin Based Systems

## EXPERIENCE:

### Graduate Research Assistant- Daniel Nocera Laboratory at Massachusetts Institute of Technology
I finished my third year as a graduate assistant in the program on a project that utilized transient absorption spectroscopy to understand the excited state dynamics of porphyrin/ acceptor systems. I completed both the synthesis of the porphyrin scaffolds and the spectroscopy on both ns and ps time resolved transient absorption systems to understand the charge separation and charge recombination rates of electron donor-acceptor systems.

### Laboratory Undergraduate Assistant- Clifford Kubiak Inorganic Laboratory at University of California San Diego
I was involved in a year of laboratory work as an undergraduate student under the guidance of several graduate students. Experiments focused on electron transfer rates between Ruthenium monomers, which are very air sensitive. Therefore, extensive lab work with schlenk glassware and glove boxes was necessary. NMR and IR techniques were used to determine mol fractions and electron transfer rates. (see publication) (April 2007-June 2008)

### Laboratory Technical Work- Los Alamos National Laboratory run by Los Alamos National Security
Hired as a technical student by a biophysics group at the lab to work with Dr. Michelle Espy and Dr. Robert Kraus, leaders of the SQUID team in Applied Modern Physics. Team worked with SQUIDS (superconducting quantum interference devices) and applications to ULF-NMR a-nd MEG imaging techniques. Maintained detailed scientific records of progress in specified projects and revitalized an otherwise stagnant Bioassay project. Was also involved in running many imaging experiments for various projects. Currently we are building a high profile liquid scanner for airports. This work is funded by the Department of Homeland Security. (June 2003-present)

### Laboratory Data Assistant- Multimodal Imaging Laboratory, Department of Neurosciences at University of California San Diego
Hired by Dr. Eric Halgren to help with image processing of various Electroencephalography (EEG) and Magnetoencephalography (MEG) studies. While employed I worked extensively with MRI/ MEG data organization and analysis and some work with SNIPS and gene analysis (October 2006- June 2007)

## Teaching—

Teaching assistant in MIT chemistry department for 1 year. Also completed the MIT Teaching Certificate Program in 2011-2012

Volunteer—Chemistry department Outreach program MIT. Assigned to go to schools and present chemistry demonstrations for middle school and high school students. Demonstrations are designed so that real life examples can be used to explain fundamental chemical concepts. (2010- 2012)

## ACTIVITIES:

Member of the chemistry REFs (Reducing and Easing Friction and Stress) program at MIT supported by the MIT mediation office.

Co-President of the Women in Chemistry program at MIT

## PUBLICATIONS:

Rates of Photoinduced Charge Separation and Charge Recombination of Axially Bound Diimide Acceptors to Zinc Tetraphenylporphyrin Hanson, C.J., Anderson, B.L., Roubelakis, M.M., Nocera, D.G. In preparation

Rates of electron self-exchange reactions between oxo-centered ruthenium clusters are determined by orbital overlap Goeltz, J. C., Hanson, C. J., Kubiak, C. P, Inorg. Chem. 2009, 48, 4763-4767.

Magnetophoresis and cytometry with magnetic microparticles International Congress Series Volume: 1300, Supplement: Complete, June, 2007, pp. 271-274 Sandin, H. ; Carr, C. ; Matlachov, A.N. ; Hanson, C.J. ; Martin, J.C. ; Ward, M.D. ; Kraus, R.H. ; Espy, M.A.

SQUID-Based Bioassay with Magnetic Particles in Flow Journal of Physics: Conference Series Volume: 43, Issue: 1, June 01, 2006, pp. 1254-1257 Espy, M A ; Carr, C ; Sandin, J H ; Hanson, C J ; Daniels, S G ; Matlachov, A N ; Graves, S W ; Ward, M D ; Jr, R H Kraus ; Fritz, S

An instrument for sorting of magnetic microparticles in a magnetic field gradient Cytometry Part A Volume: 69A, Issue: 11, 1 November 2006, pp. 1132 1142 Espy, Michelle A. ; Sandin, Henrik ; Carr, Chris ; Hanson, Christina J. ; Ward, Michael D. ; Kraus, Robert H.

Applications of ultra-low field magnetic resonance for imaging and materials studies Michelle Espy, Mark. Flynn, John Gomez, Christina Hanson, Robert Kraus, Per Magnelind, Karlene Maskaly, Andrei Matlashov, Shaun Newman, Mark Peters, Henrik Sandin, Igor Savukov, Larry Schultz, Algis Urbaitis, Petr Volegov, Vadim Zotev, Paper for Applied Superconductivity Conference August 2008

## PRESENTATIONS:

Hanson, C.J.; Anderson, B.L.; Roubelakis, M.M.; Nocera, D.G; Photoinduced Charge Transfer Between Porphyrins and Axially Bound Diimide Acceptors, 243rd National

Meeting of the American Chemical Society, San Diego, CA, March 25-29, 2012; American Chemical Society: Washington DC, 2012.

Hanson, C.J.; Kiper D.D; Nocera, D.G; Proton Coupled Electron Transfer with Iron Hangman Porphyrins, Electron Donor–Acceptor Interactions Gordon Research Conference, Newport RI, August 8-13, 2010.

Hanson, C.J.; Anderson, B.L.; Roubelakis, M.M.; Nocera, D.G; Photoinduced Charge Transfer Between Porphyrins and Axially Bound Diimide Acceptors, Electron Donor– Acceptor Interactions Gordon Research Conference, Newport RI, August 5-10, 2012.